JOURNAL OF ZOOLOGICAL SYSTEMATICS AND EVOLUTIONARY RESEARCH

Accepted on 20 July 2016
J Zool Syst Evol Res doi: 10.1111/jzs.12145

[1]*Department of Biology, Faculty of Sciences, Ferdowsi University of Mashhad, Mashhad;* [2]*Rodentology Research Department, Institute of Applied Zoology, Ferdowsi University of Mashhad, Mashhad, Iran;* [3]*Institut de Systématique, Évolution, Biodiversité ISYEB - UMR 7205 – CNRS, MNHN, UPMC, EPHE, Muséum national d'Histoire naturelle, Sorbonne Universités, Paris, France;* [4]*Zoological Innovations Research Department, Institute of Applied Zoology, Ferdowsi University of Mashhad, Mashhad, Iran*

Evolutionary history of the Persian Jird, *Meriones persicus*, based on genetics, species distribution modelling and morphometric data

Malahat Dianat[1], Jamshid Darvish[1,2,4], Raphael Cornette[3], Mansour Aliabadian[1,4] and Violaine Nicolas[3]

Abstract

The Persian Jird, *Meriones persicus*, is distributed from Eastern Anatolia to Afghanistan and western Pakistan. Six subspecies were described based on skull features and coat colours, but the validity of these subspecies is uncertain, and no molecular work has ever been conducted on this species. Iran appears to be a key geographical region in which to revise the systematic and evolutionary history of this species, because five of the six subspecies are present in this country. To evaluate the phylogeographical history and taxonomy of this species in Iran, we used a combination of genetic (cytochrome b gene sequences of 70 specimens) and geometric morphometric (2D landmarks on the ventral side of skull of 258 specimens) analyses. We also used ecological niche modelling to make inferences about the evolutionary history of these lineages. Our molecular data highlight the existence of four genetic lineages, but they only partly correspond to the previously described subspecies. Our molecular and morphometric data confirm the validity of *M. p. rossicus* and show that it has a wider geographical range than previously thought. *M. p. gurganensis* and *M. p. baptistae* are genetically very close. The skull of *M. p. gurganensis* is morphologically distinguishable from other subspecies. The subspecies *M. p. persicus* and *M. p. baptistae* are genetically distinct, but morphologically close. *Meriones p. ambrosius* is genetically close to *M. p. persicus*, and additional analyses with more specimens are needed to validate its subspecific status. The genetic structure observed in Iran seems to fit the topography and biogeography of the country and emphasize the role of the Abarkooh, Central and Lut deserts as barriers to gene flow. All intraspecific divergent events within the Persian Jird occurred during the last 1.4 My, suggesting that climatic changes probably trigger diversification within this species. Our genetic and species niche modelling results suggest that potential refugial areas persisted during glacial periods for this species in north-western Zagros Mountains, north-eastern Alborz Mountains and Kohrud Mountains.

Key words: Biogeography – cytochrome b – niche modelling – Iran – morphometry

Introduction

The Persian Jird, *Meriones persicus* (Blanford, 1875), was described from the north of Isfahan in Iran (Musser and Carleton 2005). It has been recorded from many localities in Iran, namely Mashhad, Birjand, Shirvan, Dargaz, Zoshk, Bojnord, Sabzevar, Kashmar, Gonabad, Moghan, Dasht and Kavir National Park (Goodwin 1940; Lay 1967; Brown 1980), and it is also present in Turkey (Eastern Anatolia), Iraq, Turkmenistan, Afghanistan and Pakistan (Musser and Carleton 2005). The Persian Jird inhabits rocky habitats including mountain slopes, talus and rocky outcrops (Eygelis 1980; Pavlinov et al. 1990).

Six subspecies were described within this species (Ellerman and Morrison-Scott 1951) (Fig. 1). *Meriones p. rossicus* Heptner, 1931 was described from Arzni (20 km north of Eriwan, Transcaucasia) and ranges from Turkey to Armenia and in the north-west of Iran (Ellerman and Morrison-Scott 1951; Krystufek and Vohralik 2009; Boudet 2010). *Meriones p. suschkini* Kashkarov, 1925 was described from Arshevi Les (Bashi-Mgur, Great Balkhan Mountains, Turkmenistan) and is only distributed in the Great Balkhan Mountains in the west of Turkmenistan (Ellerman and Morrison-Scott 1951; Boudet 2010). The four other subspecies are widely distributed in the Iranian Plateau. *Meriones p. baptistae* Thomas, 1920 was described from Pasht Kuh (south-west of Baluchestan) and is distributed in Pakistan (from Kelat, Kuldur, Pasht Kuh and Turbat in Baluchestan Province) and south-east of Iran (Kerman, probably from east of Zagros to south-east of Iranian Baluchestan and south of Khorasan Province) (Ellerman and Morrison-Scott 1951; Boudet 2010). *Meriones p. gurganensis* Goodwin, 1939 was described from Bojnord district and it is only known from the north-east of Iran, from Gorgan River to Kurkhud Mountains (Khorasan Province) (Ellerman and Morrison-Scott 1951; Boudet 2010). *Meriones p. persicus* Blanford, 1875, was described from Kohrud in Isfahan and is distributed from north of Isfahan to Pakistan (Ellerman and Morrison-Scott 1951; Boudet 2010). *Meriones p. ambrosius* Thomas, 1919 was described from Dopolan Mountains (Bakhtiari, 150 miles north-east of Ahwaz, Iran) and is only known from the south of Iranian Baluchestan (Ellerman 1966; Corbet 1978; Boudet 2010). All these subspecies were described based on skull features and coat colours. The taxonomy of these subspecies is under considerable discussion (Ellerman and Morrison-Scott 1951; Tabatabaei Yazdi and Adriaens 2011). The validity of these subspecies and the phylogenetic relationships among them are uncertain, and no molecular DNA study has ever been conducted on them. Iran appears to be a key geographical region to revise the systematic and evolutionary history of the Persian Jird, because five of the six subspecies are present in this country.

The earliest known *Meriones* fossil described was from Kazakhstan and is dated from the Pliocene (PDB 2011). Thus, all geological and climatic events that occurred since the Pliocene may have had a significant impact on the genetic structure of the genus. A prominent phase of tectonic deformation occurred in the Late Miocene and Early Pliocene (ca. 10–5 Mya) and led to the rise of the Iranian Plateau and new configurations of mountain ranges and drainage patterns (Homke et al. 2004; Agard et al. 2005; Mouthereau et al. 2007; Gholami et al. 2013). In the late Pliocene, the entire Zagros belt was folded and uplifted (James and Wynd 1965; Stocklin 1968). Mountains and seas acted as geographical barriers, isolating populations in different

Corresponding author: Malahat Dianat (malahatdianat2002@yahoo.com)
Contributing authors: Jamshid Darvish (Darvishj2001@yahoo.com), Raphael Cornette (cornette@mnhn.fr), Mansour Aliabadian (aliabadian@yahoo.com), Violaine Nicolas (vnicolas@mnhn.fr)

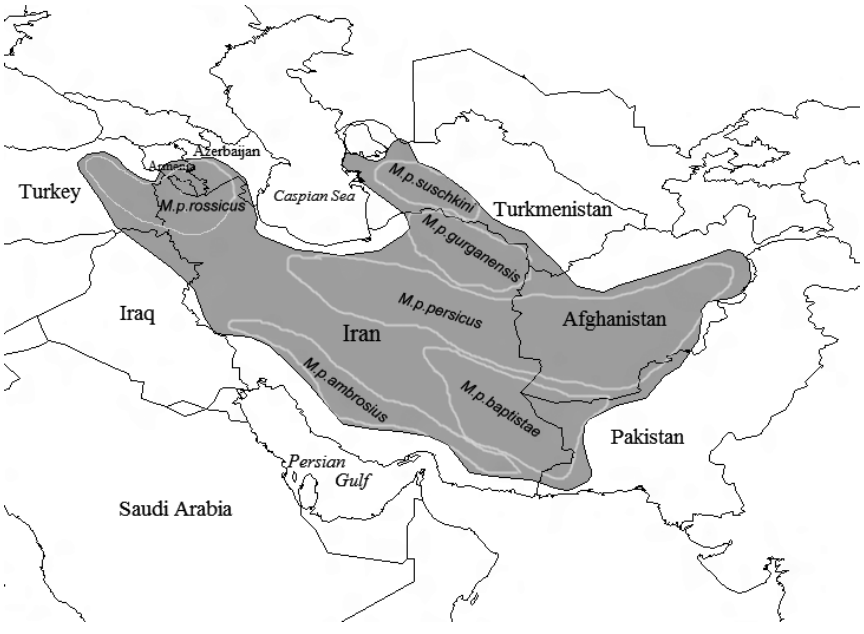

Fig. 1. Map showing the actual geographical distribution of *M. persicus* (in grey) and its subspecies based on Boudet 2010; Ellerman and Morrison-Scott 1951; Krystufek and Vohralik 2009; Ellerman 1966; Corbet 1978

glacial refugia, and constrained postglacial migration routes (Taberlet et al. 1998; Hewitt 1999). Quaternary climatic fluctuations shaped the genetic diversity of terrestrial biota throughout the Holarctic (Hewitt 2000). The possible influence of the Pleistocene climatic fluctuations and the glaciations on the Iranian biota has not been investigated before. In Iran, the conditions during the glacial periods were colder and more arid than present conditions, resulting in extended deserts and steppe and reduced warm wet habitats (Djamali et al. 2008; Kehl 2009; Langgut et al. 2011; Rajaei et al. 2013). The last interglacial period appears to have been slightly warmer and moister than the Holocene, which favoured forest vegetation (Djamali et al. 2008). Topographical complexity has made the Middle East, and Iran in particular, a likely place for multiple refugia, where genetic diversity may have accumulated over several glacial periods, leading to the origin of new lineages and ultimately new taxa (Gvozdik et al. 2010). The refugial and speciation properties of the mountains derive from their topographic variety, which allows habitats and lineages to persist by altitudinal shifts and also to diverge because of distributional dissection.

To evaluate the phylogeographical history and taxonomy of the species *M. persicus*, we used a combination of genetic and geometric morphometric (GM) analyses. For the molecular analyses, we used the *cytochrome b* gene (*cyt b*), as it is the most widely used mitochondrial DNA marker for resolving phylogenetic relationships and for inferring species boundaries in rodents (Castresana 2001). Geometric morphometrics is a statistically powerful and visually effective method to solve systematic difficulties (Bookstein 1991; Rohlf and Marcus 1993; Adams et al. 2004; Cardini and Elton 2009; Zelditch et al. 2012). The use of landmark data to quantify the variation in both skull size and shape in mammals is sufficiently powerful to resolve issue where even the subtle variation is at hand (Rohlf and Marcus 1993; Fadda and Corti 2000; Barciova and Macholan 2006; Cardini et al. 2007; Macholan et al. 2008; Cardini and Elton 2009). We also used ecological niche modelling to make inferences about the evolutionary history of these lineages. This study aimed to (1) define subspecies limits within *M. persicus,* using molecular and GM data, (2) test whether large deserts (Abarkooh, Central and Lut deserts) have acted as significant barriers to gene flow through time in this species and (3) test the role of mountains as long-standing refugia for this species during Pleistocene glacial cycles.

Materials and Methods

Molecular analyses

DNA extraction and amplification

DNA was extracted from frozen muscles or the heart (Bruford et al. 1992), amplified and sequenced following the methods described in Chevret et al. (2005) and Aliabadian et al. (2007). The primer pairs L7 (5′-ACT AAT GAC ATG AAA AATCAT CGT T-3′) and H6 (5′-TCT TCA TTT TTG GTT TAC AAGAC-3′) were used for both polymerase chain reaction (PCR) amplification and cycle sequencing (Montgelard et al. 2002). The *cytochrome b (cyt b)* gene was sequenced for 70 individuals, and the sequences were submitted to GenBank (Fig. 2, Table 1).

Phylogenetic analyses

The sequences were aligned automatically with BIOEDIT (Hall 1999). Each alignment was then edited by eye.

Phylogenetic relationships were analysed by maximum-likelihood analyses (software phyML, Guindon et al. 2010). We chose the mutation model that best fitted the data according to the Akaike information criterion (Akaike 1973) using MrModeltest 3.7 (Posada and Crandall 2001a). Node support was estimated by bootstrap analysis with 100 replications, and the BIONJ distance-based tree was used as the starting tree. Fifteen taxa were used as outgroups for this analysis: *Meriones vinogradovi* (GenBank KU561098), *M. grandis* (KM581508), *M. shawi* (KM581620), *M. crassus* (AJ851267), *M. rex* (AJ851265), *M. tristrami* (KU561099), *M. libycus* (JQ927411), *M. chengi* (AB381900), *M. meridianus* (AJ8512 68), *M. unguiculatus* (AF119264), *Psammomys obesus* (AJ851275), *Rhombomys opimus* (AJ430556), *Gerbillus gerbillus* (AJ851269), *Sekeetamys calurus* (AJ851276) and *Tatera indica* (AJ430563).

Divergence time estimates

Divergence time estimates were inferred using BEAST v.1.8 package (Drummond and Rambaut 2007) under an uncorrelated lognormal relaxed clock, which allows independent rates of nucleotide substitution on different branches. BEAST uses Markov chain Monte Carlo to approximate time-calibrated phylogenies along with credibility intervals. We chose the DNA substitution model that fit the data best, according to the Akaike information criterion (Akaike 1973), using MrModeltest v 3.7 (Posada

doi: 10.1111/jzs.12145

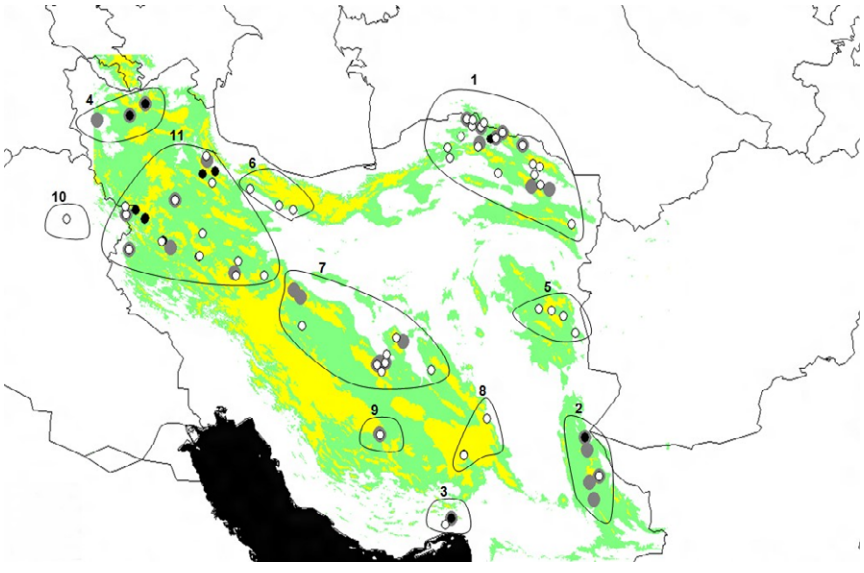

Fig. 2. Map showing the sampling points (white ovals: localities with specimens only included in morphometric analyses, black ovals: localities with specimens only included in molecular analyses, grey ovals: localities with specimens included in both morphometric and molecular analyses) and the 11 groups used for geometric morphometric analyses. These groups were defined based on subspecies range according to bibliographical data, genetic results and geographical origin of specimens. Colours indicate altitude: white: altitude below 1270 m; green: altitude between 1270 and 2000 m; yellow: altitude higher than 2000 m

and Crandall 2001a). We used a coalescent Bayesian Skyline model that allows us to reconstruct the changes in population sizes through time (Drummond et al. 2005). We run two independent replicates, each consisting of 100 000 000 generations, with trees sampled every 10 000 generations.

They were then combined in TRACER version 1.4 (Rambaut et al. 2013), which also provides options for examining effective sample size values (all ESS values were larger than 200, which is considered as adequate, according to the BEAST tutorial) and frequency plots to check that mixing of the MCMC chain was adequate. The majority consensus and posterior probabilities (PP) for each node were calculated from the trees after the first 25% of the trees were discarded as the 'burn-in' (i.e. trees sampled before the chains had reached stationarity). Four fossil calibrations were used to calibrate the chronogram. All calibrations were applied as lognormal prior distributions, and the means and standard deviations of these distributions were chosen to construct 95% confidence intervals that spanned the 90–95% Marshall indices (Marshall 1994) reported by the Paleobiology Database (Jaeger et al. 1986; PDB 2011). These represent the 95% estimated confidence interval, for the origination of a taxon based on first occurrences and stratigraphic sampling. The first two calibrations applied to the phylogeny have been used in previous studies (Schenk et al. 2013; Alhajeri et al. 2015): (1) the Gerbillinae–Deomyinae split based on the first occurrence of Gerbillinae in the Lower Miocene fauna of Saudi Arabia (offset = 15.8, range = 16.0–23.7); (2) the *Lophuromys–Acomys–Deomys* split, hence indicating the origin of *Acomys*, based on the earliest known *Acomys* fossil from Kenya (offset = 5.2, range = 5.3–29.0); (3) the *Meriones–Psammomys–Rhombomys* split, hence indicating the origin of *Meriones*, based on the earliest known *Meriones* fossil from Kazakhstan in the Pliocene (offset = 2.6, range = 2.6–5.3); (4) the *Gerbillus–Sekeetamys* split based on the first occurrence of the genus *Gerbillus* in Armenia in the Pliocene (offset = 2.6; range = 2.6–5.3). We used a log-normal relaxed molecular clock model (Drummond et al. 2006). The following species were used as outgroups: *Mus musculus* (AB819920), *Uranomys ruddi* (HM635858), *Acomys airensis* (AJ012021), *A. cahirinus* (AJ233953), *A. chudeaui* (FJ415538), *A. cilicicus* (AJ233957), *A. dimidiatus* (AJ233959), *A. ignitus* (Z96064), *A. johannis* (HM635823), *A. minous* (GU046553), *A. nesiotes* (AJ233952), *A. percivali* (EF187818), *A. russatus* (FJ415485), *A. spinosissimus* (AM409396), *A. subspinosus* (JN247673), *A. wilsoni* (EF187799), *Deomys ferrugineus* (FJ415478), *Lophuromys flavopunctatus* (EU349754), *L. sikapusi* (AJ012023), *Desmodillus auricularis* (AJ851272), *Gerbilliscus robustus* (AM409374), *G. guinea* (AJ430562), *Gerbillurus paeba* (AJ430557), *G. tytonis* (AJ430559), *Sekeetamys calurus* (AJ851276), *Gerbillus campestris* (AJ851271), *G. gerbillus* (AJ851269), *G. henleyi* (JQ753050), *G. nanus* (JQ753051), *G. poecilops* (JQ753064), *G. simoni* (GU356577), *G. tarabuli* (GU356573), *Desmodilliscus braueri* (AJ851273), *Taterillus arenarius* (AJ851261), *Psammomys obesus* (AJ851275), *Rhombomys opimus* (AJ430556), *Meriones vinogradovi* (KU561098), *M. grandis* (KM581508), *M. shawi* (KM581620), *M. chengi* (AB381900), *M. crassus* (AJ851267), *M. libycus* (JQ927411), *M. meridianus* (AJ851268), *M. rex* (AJ851265), *M. unguiculatus* (AF119264) and *M. tristrami* (KU561099).

Intraspecific gene evolution cannot always be represented by a bifurcating tree. Rather, population genealogies are often multifurcated, descendant genes coexist with persistent ancestors and recombination events produce reticulate relationships (Posada and Crandall 2001b). Networking approaches taking into account these population-level phenomena are thus suitable to infer intraspecific gene genealogies. Phylogenetic relationships between haplotypes were also inferred by constructing a network using the median-joining method available in NETWORK, version 4.500 (Bandelt et al. 1999).

Genetic diversity, genetic structure and demographic history

Genetic distances between lineages were calculated using the Kimura 2-parameter (K2P) model of evolution (Kimura 1980), as implemented in MEGA v 4.0 (Tamura et al. 2007). The choice of this model allowed us to compare our values to those in the literature. Several reference values are available for the *cyt b* marker concerning intra- and interspecific divergence values among rodents, so we could test the specific status of each lineage under the genetic species concept. Where applicable, we estimated several statistics to describe and compare the major lineages recovered from our phylogenetic analyses. The number of polymorphic sites, average number of nucleotide differences, nucleotide diversity and haplotype diversity were calculated for each lineage using DNASP v 5.10 (Librado and Rozas 2009). We assessed the population history using two statistics that were introduced as tests for neutrality but that are also capable of detecting the genetic traces of population growth, decline or stability: Tajima's D (Tajima 1989) and Fu's Fs test (Fu 1997). Population expansions lead to significant negative departures of D and Fs values from zero. These analyses were performed with ARLEQUIN v 3.11 (Excoffier et al. 2005), and their significance was assessed using 1000 coalescent simulations. As suggested in the ARLEQUIN manual, the Fs ad D statistics were considered significant when $p < 0.02$ and $p < 0.05$, respectively. We also used a test based on mismatch distributions in each

doi: 10.1111/jzs.12145

Table 1. List of specimens used in this study, with voucher numbers, localities of collect (for specimens included in genetic analyses, numbers in parentheses refer to localities numbers in Fig. 5), genetic lineages (numbers after '/' refer to the haplotype number in Fig. 4), GenBank accession numbers, morphometric data sets and groups. ZMFUM: Zoology Museum of Ferdowsi University of Mashhad, Mashhad, Iran. MNHN: French National Museum of Natural History, Paris, France.

Voucher No.	Country-Province-Locality	mt Lineages	Accession number	Data set/groups
MNHN ZM-MO1950-423	Iran-Azarbayejan Gharbi, Naghade			A-B-C/4
MNHN ZM-MO1950-429	Iran-Azarbayejan Gharbi, Naghade			A-B-C/4
MNHN ZM-MO1950-435	Iran-Azarbayejan Gharbi, Naghade			A-B-C/4
MNHN ZM-MO1950-437	Iran-Azarbayejan Gharbi, Naghade			A-B-C/4
ZMFUM4347	Iran-Azarbayejan Gharbi, Orumie (14)	IA/27	KT949975	A-B-C/4
ZMFUM2212	Iran-Azarbayejan Sharghi-Jolfa, Kordasht (11)	IA/30	KT949996	
ZMFUM2214	Iran-Azarbayejan Sharghi-Jolfa, Kordasht (11)	IA/29	KT949997	
ZMFUM2220	Iran-Azarbayejan Sharghi-Jolfa, Kordasht (11)	IA/31	KT949998	
ZMFUM2223	Iran-Azarbayejan Sharghi-Jolfa, Kordasht (11)	IA/30	KT949999	A-B-C/4
ZMFUM2999	Iran-Azarbayejan Sharghi-Jolfa, Kordasht (11)	IA/28	KT949991	
ZMFUM2208	Iran-Azarbayejan Sharghi-Tabriz, SaddeAmand (10)	IA/27	KT949994	
ZMFUM2209	Iran-Azarbayejan Sharghi-Tabriz, Sadde Amand (10)	IA/27	KT949995	
ZMFUM2224	Iran-Azarbayejan Sharghi-Tabriz, Sadde Amand (10)	IA/36	KT949990	A-B-C/4
ZMFUM2909	Iran-Azarbayejan Sharghi-Tabriz, Sadde Amand (10)	IA/30	KT949986	
ZMFUM2910	Iran-Azarbayejan Sharghi-Tabriz, Sadde Amand (10)	IA/30	KT949987	
MNHN ZM-MO1985-1628	Iran-Esfahan, Esfahan			A-B/7
ZMFUM4516	Iran-Esfahan-Moorche Khort, Lamoosh (33)	IIB/6	KT949953	A-B-C/7
ZMFUM4527	Iran-Esfahan-Moorche Khort, Lamoosh (33)	IIB/2	KT949951	A-B-C/7
ZMFUM4517	Iran-Esfahan-Moorche Khort, Patili (32)	IIB/1	KT949952	A-B-C/7
ZMFUM4522	Iran-Esfahan-Moorche Khort, Patili (32)	IIB/2	KT949950	A-B-C/7
MNHN ZM-MO1957-982	Iran-Ghazvin, Ghazvin			A-B-C/6
MNHN ZM-MO1957-984	Iran-Ghazvin, Ghazvin			A-B-C/6
MNHN ZM-MO1957-985	Iran-Ghazvin, Ghazvin			A-B-C/6
MNHN ZM-MO1957-986	Iran-Ghazvin, Ghazvin			A-B-C/6
MNHN ZM-MO1957-988	Iran-Ghazvin, Ghazvin			A-B-C/6
MNHN ZM-MO1957-989	Iran-Ghazvin, Ghazvin			A-B-C/6
MNHN ZM-MO1957-990	Iran-Ghazvin, Ghazvin			A-B-C/6
MNHN ZM-MO1957-991	Iran-Ghazvin, Ghazvin			A-B-C/6
ZMFUM4213	Iran-Hamedan, Hamedan			A-B/11
MNHN ZM-MO1952-515	Iran-Hamedan-Tuyserkan, Malitche			A-B-C/11
ZMFUM4502	Iran-Hormozgan-Bandarabas, Geno			A/3
ZMFUM4514	Iran-Hormozgan-Bandarabas, Khoorgoo (31)	IIB/49	KT949956	A/3
ZMFUM4515	Iran-Hormozgan-Bandarabas, Khoorgoo (31)	IIB/49	KT949974	
ZMFUM4424	Iran-Kerman, Anar			A-B/8
ZMFUM4426	Iran-Kerman, Anar			A-B/8
ZMFUM4430	Iran-Kerman, Anar			A-B/8
ZMFUM4435	Iran-Kerman, Anar			A-B/8
ZMFUM4443	Iran-Kerman, Anar			A-B/8
ZMFUM4462	Iran-Kerman, Anar			A-B-C/8
ZMFUM4432	Iran-Kerman-Baft, Niazabad			A-B/8
ZMFUM4433	Iran-Kerman-Baft, Niazabad			A-B/8
ZMFUM4439	Iran-Kerman-Baft, Niazabad			A-B/8
ZMFUM4440	Iran-Kerman-Baft, Niazabad			A-B/8
ZMFUM4446	Iran-Kerman-Baft, Niazabad			A-B/8
ZMFUM4453	Iran-Kerman-Baft, Niazabad			A-B/8
ZMFUM4458	Iran-Kerman-Baft, Niazabad			A-B-C/8
ZMFUM4412	Iran-Kerman-Rafsanjan, Taj abad			A-B/8
ZMFUM4413	Iran-Kerman-Rafsanjan, Taj abad			A-B/8
ZMFUM4414	Iran-Kerman-Rafsanjan, Taj abad			A-B/8
ZMFUM4415	Iran-Kerman-Rafsanjan, Taj abad			A-B/8
ZMFUM4416	Iran-Kerman-Rafsanjan, Taj abad			A-B/8
ZMFUM4417	Iran-Kerman-Rafsanjan, Taj abad			A-B/8
ZMFUM4419	Iran-Kerman-Rafsanjan, Taj abad			A-B/8
ZMFUM4420	Iran-Kerman-Rafsanjan, Taj abad			A-B-C/8
ZMFUM4422	Iran-Kerman-Rafsanjan, Taj abad			A-B/8
ZMFUM4423	Iran-Kerman-Rafsanjan, Taj abad			A-B/8
ZMFUM4428	Iran-Kerman-Rafsanjan, Taj abad			A-B/8
ZMFUM4429	Iran-Kerman-Rafsanjan, Taj abad			A-B/8
ZMFUM4431	Iran-Kerman-Rafsanjan, Taj abad			A-B/8
ZMFUM4434	Iran-Kerman-Rafsanjan, Taj abad			A-B/8
ZMFUM4437	Iran-Kerman-Rafsanjan, Taj abad			A-B/8
ZMFUM4438	Iran-Kerman-Rafsanjan, Taj abad			A-B/8
ZMFUM4447	Iran-Kerman-Rafsanjan, Taj abad			A-B/8
ZMFUM4450	Iran-Kerman-Rafsanjan, Taj abad			A-B/8
ZMFUM4452	Iran-Kerman-Rafsanjan, Taj abad			A-B/8
ZMFUM4455	Iran-Kerman-Rafsanjan, Taj abad			A-B/8
ZMFUM4459	Iran-Kerman-Rafsanjan, Taj abad			A-B/8
ZMFUM4466	Iran-Kerman-Rafsanjan, Taj abad			A-B/8

doi: 10.1111/jzs.12145

Table 1. (continued)

Voucher No.	Country-Province-Locality	mt Lineages	Accession number	Data set/groups
ZMFUM317	Iran-Kerman, Toonel Sirch			A-B/8
MNHN ZM-MO1950-436	Iran-Kermanshah-Kamyaran, Samele			A-B-C/11
MNHN ZM-MO1950-438	Iran-Kermanshah-Kamyaran, Samele			A-B-C/11
MNHN ZM-MO1950-440	Iran-Kermanshah-Kamyaran, Samele			A-B-C/11
MNHN ZM-MO1950-442	Iran-Kermanshah-Kamyaran, Samele			A-B-C/11
ZMFUM3997	Iran-Kermanshah, Songhor (6)	IA/39	KT949979	
ZMFUM527	Iran-Khorasan Jonoobi-Birjand, Asadiye			A-B-C/5
ZMFUM654	Iran-Khorasan Jonoobi-Birjand, Darmian			A-B-C/5
ZMFUM843	Iran-Khorasan Jonoobi-Birjand, Kalate Bazdid			A-B-C/5
ZMFUM558	Iran-Khorasan Jonoobi-Birjand, Mansurabad			A-B-C/5
ZMFUM767	Iran-Khorasan Jonoobi-Birjand, Mansurabad			A-B-C/5
ZMFUM478	Iran-Khorasan Jonoobi-Birjand, Sarasiab			A-B-C/5
ZMFUM498	Iran-Khorasan Jonoobi-Birjand, Sarasiab			A-B-C/5
ZMFUM2655	Iran-Khorasan Razavi, Chenaran			A-B-C/1
ZMFUM2852	Iran-Khorasan Razavi, Chenaran (25)	IIA/24	KT949964	A-B-C/1
ZMFUM3183	Iran-Khorasan Razavi, Chenaran			A-B-C/1
ZMFUM3748	Iran-Khorasan Razavi, Chenaran			A-B-C/1
ZMFUM3752	Iran-Khorasan Razavi, Chenaran			A-B-C/1
ZMFUM3755	Iran-Khorasan Razavi, Chenaran			A-B-C/1
ZMFUM3804	Iran-Khorasan Razavi, Chenaran			A-B-C/1
ZMFUM3853	Iran-Khorasan Razavi, Chenaran			A-B-C/1
ZMFUM3859	Iran-Khorasan Razavi, Chenaran			A-B-C/1
ZMFUM3860	Iran-Khorasan Razavi-Chenaran, Boghmech			A-B-C/1
ZMFUM3861	Iran-Khorasan Razavi-Chenaran, Boghmech			A-B-C/1
ZMFUM3867	Iran-Khorasan Razavi-Chenaran, Boghmech			A-B-C/1
ZMFUM3868	Iran-Khorasan Razavi-Chenaran, Boghmech			A-B-C/1
ZMFUM3931	Iran-Khorasan Razavi-Chenaran, Boghmech			A-B-C/1
ZMFUM3966	Iran-Khorasan Razavi-Chenaran, Boghmech			A-B-C/1
ZMFUM3970	Iran-Khorasan Razavi-Chenaran, Boghmech			A-B-C/1
ZMFUM3993	Iran-Khorasan Razavi-Chenaran, Boghmech			A-B-C/1
ZMFUM1237	Iran-Khorasan Razavi-Mashhad, Khajeh Morad (23)	IIA/23	KT949959	A-B-C/1
ZMFUM1455	Iran-Khorasan Razavi-Mashhad, Zoshk			A-B-C/1
ZMFUM2174	Iran-Khorasan Razavi-Neyshaboor, Soomee (17)	IIA/26	KT949968	A-B-C/1
ZMFUM2177	Iran-Khorasan Razavi-Neyshaboor, Soomee (17)	IIA/26	KT949969	A-B-C/1
ZMFUM1109	Iran-Khorasan Razavi, Tandure (21)	IIA/19	KT949957	A-B/1
ZMFUM1111	Iran-Khorasan Razavi, Tandure			A-B/1
ZMFUM1112	Iran-Khorasan Razavi, Tandure			A-B/1
ZMFUM1113	Iran-Khorasan Razavi, Tandure (21)	IIA/24	KT949958	A-B-C/1
ZMFUM1114	Iran-Khorasan Razavi, Tandure			A-B-C/1
ZMFUM1116	Iran-Khorasan Razavi, Tandure			A-B-C/1
ZMFUM372	Iran-Khorasan Razavi-Torbat, Bidestan			A-B-C/1
ZMFUM2912	Iran-Khorasan Shomali, Baghlegh			A-B-C/1
ZMFUM2916	Iran-Khorasan Shomali, Baghlegh (28)	IIA/18	KT949961	A-B-C/1
ZMFUM2917	Iran-Khorasan Shomali, Baghlegh (28)	IIA/17	KT949962	
ZMFUM2966	Iran-Khorasan Shomali, Baghlegh			A-B-C/1
ZMFUM2995	Iran-Khorasan Shomali, Baghlegh			A-B-C/1
ZMFUM2843	Iran-Khorasan Shomali-Bojnord, Ayoob			A-B-C/1
ZMFUM2888	Iran-Khorasan Shomali-Bojnord, Ayoob (29)	IIA/21	KT949966	A-B-C/1
ZMFUM2927	Iran-Khorasan Shomali-Bojnord, Gifan			A-B-C/1
ZMFUM2934	Iran-Khorasan Shomali-Bojnord, Gifan			A-B/1
ZMFUM2935	Iran-Khorasan Shomali-Bojnord, Gifan			A-B-C/1
ZMFUM3174	Iran-Khorasan Shomali-Bojnord, Jajarm			A-B-C/1
ZMFUM3188	Iran-Khorasan Shomali-Bojnord, Jajarm			A-B-C/1
ZMFUM3222	Iran-Khorasan Shomali-Bojnord, Mahnan			A-B-C/1
MNHN ZM-MO1957-1351	Iran-Khorasan Shomali-Bojnord, Robat Qarabil			A-B-C/1
ZMFUM2639	Iran-Khorasan Shomali-Esfarayen, Kale Shoor			A-B-C/1
ZMFUM3606	Iran-Khorasan Shomali-Esfarayen, Kale Shoor			A-B-C/1
ZMFUM3652	Iran-Khorasan Shomali-Esfarayen, Kale Shoor			A-B-C/1
ZMFUM3668	Iran-Khorasan Shomali-Esfarayen, Kale Shoor			A-B-C/1
ZMFUM3669	Iran-Khorasan Shomali-Esfarayen, Kale Shoor			A-B-C/1
ZMFUM3673	Iran-Khorasan Shomali-Esfarayen, Kale Shoor			A-B-C/1
ZMFUM3674	Iran-Khorasan Shomali-Esfarayen, Kale Shoor			A-B-C/1
ZMFUM2972	Iran-Khorasan Shomali, Mane Samalghan			A-B-C/1
ZMFUM2925	Iran-Khorasan Shomali, Razo jargalan (24)	IIA/20	KT949960	A-B-C/1
ZMFUM2996	Iran-Khorasan Shomali, Razo jargalan			A-B-C/1
ZMFUM2983	Iran-Khorasan Shomali-Razo jargalan, Gholaman			A-B-C/1
ZMFUM3001	Iran-Khorasan Shomali-Razo jargalan, Gholaman			A-B-C/1
ZMFUM3002	Iran-Khorasan Shomali-Razo jargalan, Gholaman			A-B-C/1
ZMFUM3019	Iran-Khorasan Shomali-Razo jargalan, Gholaman			A-B/1
ZMFUM4969	Iran-Khorasan Shomali, Shirvan (26)	IIA/22	KT949967	
ZMFUM2924	Iran-Khorasan Shomali-Shirvan, Ghoolanloo (27)	IIA/19	KT949963	A-B-C/1

doi: 10.1111/jzs.12145

Table 1. (continued)

Voucher No.	Country-Province-Locality	mt Lineages	Accession number	Data set/groups
ZMFUM3120	Iran-Khorasan Shomali-Shirvan, Ghoolanloo			A-B-C/1
ZMFUM3182	Iran-Khorasan Shomali-Shirvan, Ghoolanloo			A-B-C/1
ZMFUM3193	Iran-Khorasan Shomali-Shirvan, Ghoolanloo			A-B-C/1
ZMFUM3260	Iran-Khorasan Shomali-Shirvan, Ghoolanloo			A-B-C/1
ZMFUM3262	Iran-Khorasan Shomali-Shirvan, Ghoolanloo			A-B-C/1
ZMFUM3270	Iran-Khorasan Shomali-Shirvan, Ghoolanloo			A-B-C/1
ZMFUM2631	Iran-Khorasan Shomali-Shirvan, Golool			A-B-C/1
ZMFUM2637	Iran-Khorasan Shomali-Shirvan, Golool			A-B-C/1
ZMFUM2661	Iran-Khorasan Shomali-Shirvan, Golool			A-B-C/1
ZMFUM2874	Iran-Khorasan Shomali-Shirvan, Golool			A-B-C/1
ZMFUM2885	Iran-Khorasan Shomali-Shirvan, Golool (22)	IIA/25	KT949965	A-B-C/1
ZMFUM4348	Iran-Kordestan, Bijar (15)	IA/45	KT949977	A-B-C/11
ZMFUM4349	Iran-Kordestan, Bijar (15)	IA/33	KT949978	A-B-C/11
ZMFUM4350	Iran-Kordestan, Bijar			A-B-C/11
ZMFUM4351	Iran-Kordestan, Bijar			A-B-C/11
ZMFUM4093	Iran-Kordestan, Marivan			A-B/11
ZMFUM4094	Iran-Kordestan, Marivan			A-B/11
ZMFUM4964	Iran-Kordestan-Marivan, Ghamishleh (12)	IA/34	KT949981	
ZMFUM4558	Iran-Kordestan-Marivan, Pasgahe Marzi (8)	IA/41	KT949982	A-B-C/11
ZMFUM4967	Iran-Kordestan-Marivan, Pasgahe Marzi (8)	IA/41	KT949989	
ZMFUM3904	Iran-Kordestan, Saghez			A-B-C/11
ZMFUM3919	Iran-Kordestan, Saghez			A-B-C/11
ZMFUM3921	Iran-Kordestan, Saghez (4)	IA/35	KT950000	A-B-C/11
ZMFUM3922	Iran-Kordestan, Saghez (4)	IA/42	KT949980	A-B-C/11
ZMFUM3923	Iran-Kordestan, Saghez			A-B-C/11
ZMFUM3924	Iran-Kordestan, Saghez			A-B-C/11
ZMFUM3929	Iran-Kordestan, Saghez			A-B-C/11
ZMFUM3930	Iran-Kordestan, Saghez			A-B-C/11
ZMFUM4000	Iran-Kordestan, Saghez			A-B-C/11
ZMFUM4002	Iran-Kordestan, Saghez			A-B-C/11
ZMFUM4556	Iran-Kordestan, Saghez			A-B/11
ZMFUM4557	Iran-Kordestan, Saghez			A-B/11
ZMFUM4559	Iran-Kordestan, Saghez			A-B/11
MNHN ZM-MO1949-284	Iran-Kordestan, Saghez			A-B/11
ZMFUM4016	Iran-Kordestan-Sanandaj, Ghaderabad (5)	IA/33	KT949985	
ZMFUM4965	Iran-Kordestan-Sanandaj, Ghaderabad (5)	IA/32	KT949984	
ZMFUM4968	Iran-Kordestan-Sanandaj, Ghaderabad (5)	IA/37	KT949983	
ZMFUM3902	Iran-Kordestan, Songhor (13)	IA/33	KT949992	A-B-C/11
ZMFUM3928	Iran-Kordestan, Songhor (13)	IA/33	KT949976	A-B-C/11
ZMFUM4060	Iran-Markazi-Arak, Gardane Sibak			A-B/11
ZMFUM4059	Iran-Markazi-Arak, Mashhadolkoobe			A-B/11
ZMFUM4066	Iran-Markazi-Arak, Namak Koor (3)	IA/46	KT949993	A-B/11
MNHN ZM-MO1957-977	Iran-Markazi, Mahallat			A-B-C/11
MNHN ZM-MO1957-979	Iran-Markazi, Mahallat			A-B-C/11
ZMFUM3279	Iran-Sistan Baluchestan-Khaash, Aab Khan (18)	IIA/12	KT950005	A-B-C/2
ZMFUM3280	Iran-Sistan Baluchestan-Khaash, Aab Khan (18)	IIA/14	KT950013	A-B/2
ZMFUM3301	Iran-Sistan Baluchestan, Taftan (30)	IIA/13	KT950008	A-B-C/2
ZMFUM3525	Iran-Sistan Baluchestan-Zahedan, Koole Sangi (20)	IIA/15	KT950006	A-B/2
ZMFUM3526	Iran-Sistan Baluchestan-Zahedan, Koole Sangi (20)	IIA/15	KT950014	
ZMFUM3972	Iran-Sistan Baluchestan-Zahedan, Manzel Aab (16)	IIA/11	KT950007	A-B-C/2
ZMFUM3973	Iran-Sistan Baluchestan-Zahedan, Manzel Aab (16)	IIA/11	KT950009	A-B-C/2
ZMFUM3985	Iran-Sistan Baluchestan-Zahedan, Manzel Aab (16)	IIA/11	KT950012	A-B-C/2
ZMFUM3680	Iran-Sistan Baluchestan-Zahedan, Mirjave Tamin (19)	IIA/12	KT950011	
ZMFUM3684	Iran-Sistan Baluchestan-Zahedan, Mirjave Tamin			A-B/2
ZMFUM3685	Iran-Sistan Baluchestan-Zahedan, Mirjave Tamin			A-B/2
ZMFUM3694	Iran-Sistan Baluchestan-Zahedan, Mirjave Tamin (19)	IIA/12	KT950010	A-B/2
ZMFUM3695	Iran-Sistan Baluchestan-Zahedan, Mirjave Tamin (19)	IIA/16	KT950015	A-B/2
MNHN ZM-MO1947-848	Iran-Tehran, Hesarak			A-B-C/6
ZMFUM1393	Iran-Tehran, Tehran			A-B-C/6
ZMFUM1395	Iran-Tehran, Tehran			A-B-C/6
ZMFUM1396	Iran-Tehran, Tehran			A-B-C/6
ZMFUM1397	Iran-Tehran, Tehran			A-B-C/6
ZMFUM1398	Iran-Tehran, Tehran			A-B-C/6
ZMFUM4565	Iran-Yazd, Bafgh			A-B/7
ZMFUM4567	Iran-Yazd, Bafgh			A-B/7
ZMFUM4568	Iran-Yazd, Bafgh			A-B/7
ZMFUM4569	Iran-Yazd, Bafgh			A-B/7
ZMFUM4571	Iran-Yazd, Bafgh			A-B/7
ZMFUM4574	Iran-Yazd, Bafgh			A-B-C/7
ZMFUM4575	Iran-Yazd, Bafgh			A-B-C/7
ZMFUM3535	Iran-Yazd-Khaatam, Baghe Shadi (1)	IB/48	KT950016	A-C/9

doi: 10.1111/jzs.12145

Table 1. (continued)

Voucher No.	Country-Province-Locality	mt Lineages	Accession number	Data set/groups
ZMFUM3546	Iran-Yazd-Khaatam, Baghe Shadi (1)	IB/47	KT950017	A-C/9
ZMFUM1301	Iran-Yazd, Kharanagh			A-B/7
ZMFUM1376	Iran-Yazd-Kharanagh, Nafisabad (37)	IIB/7	KT949972	A-B/7
ZMFUM1619	Iran-Yazd-Kharanagh, Nafisabad (37)	IIB/8	KT949955	A-B-C/7
ZMFUM3810	Iran-Yazd-Mehriz			A-B-C/7
ZMFUM1519	Iran-Yazd, Shirkooh (36)	IIB/3	KT949948	A-B/7
ZMFUM2956	Iran-Yazd, Shirkooh			A-B-C/7
ZMFUM2970	Iran-Yazd, Shirkooh			A-B-C/7
ZMFUM3055	Iran-Yazd, Shirkooh			A-B-C/7
ZMFUM3834	Iran-Yazd-Shirkooh, Baghe Mahdi (34)	IIB/5	KT949954	A-B-C/7
ZMFUM1706	Iran-Yazd-Taft, Eslamiye			A-B-C/7
ZMFUM1707	Iran-Yazd-Taft, Eslamiye			A-B-C/7
ZMFUM1708	Iran-Yazd-Taft, Eslamiye			A-B-C/7
ZMFUM1710	Iran-Yazd-Taft, Dare Gahan (35)	IIB/4	KT949949	A-B-C/7
ZMFUM3749	Iran-Yazd-Taft, Dare Gahan (35)	IIB/9	KT949970	A-B-C/7
ZMFUM3750	Iran-Yazd-Taft, Dare Gahan (35)	IIB/9	KT949971	A-B-C/7
ZMFUM3751	Iran-Yazd-Taft, Dare Gahan (35)	IIB/10	KT949973	A-B-C/7
ZMFUM3731	Iran-Yazd-Taft, Sange Deraz			A-B-C/7
ZMFUM3811	Iran-Yazd-Taft, Sange Deraz			A-B-C/7
ZMFUM1620	Iran-Yazd, Yazd			A-B-C/7
ZMFUM1700	Iran-Yazd, Yazd			A-B-C/7
ZMFUM3023	Iran-Yazd, Yazd			A-B-C/7
ZMFUM3035	Iran-Yazd, Yazd			A-B-C/7
ZMFUM3549	Iran-Yazd, Yazd			A-B-C/7
MNHN ZM-MO1950-424	Iran-Zanjan, Soltanieh			A-B-C/11
ZMFUM1566	Iran-Zanjan, Sorkhabad			A-B-C/11
ZMFUM1638	Iran-Zanjan, Sorkhabad (7)	IA/38	KT950003	A-B-C/11
ZMFUM2210	Iran-Zanjan, Zanjan (9)	IA/40	KT950004	
ZMFUM2213	Iran-Zanjan, Zanjan (9)	IA/40	KT950001	
ZMFUM4210	Iran-Zanjan-Zanjan, Amirabad (2)	IA/44	KT950002	
ZMFUM4212	Iran-Zanjan-Zanjan, Amirabad (2)	IA/43	KT949988	
MNHN ZM-MO1957-282	Iraq-Kirkuk-Kirkuk, Mullaabdolah			A-B-C/10
MNHN ZM-MO1957-283	Iraq-Kirkuk-Kirkuk, Mullaabdolah			A-B-C/10
MNHN ZM-MO1957-285	Iraq-Kirkuk-Kirkuk, Mullaabdolah			A-B-C/10
MNHN ZM-MO1957-286	Iraq-Kirkuk-Kirkuk, Mullaabdolah			A-B-C/10
MNHN ZM-MO1957-287	Iraq-Kirkuk-Kirkuk, Mullaabdolah			A-B-C/10
MNHN ZM-MO1957-288	Iraq-Kirkuk-Kirkuk, Mullaabdolah			A-B-C/10
MNHN ZM-MO1957-290	Iraq-Kirkuk-Kirkuk, Mullaabdolah			A-B-C/10
MNHN ZM-MO1957-291	Iraq-Kirkuk-Kirkuk, Mullaabdolah			A-B-C/10
MNHN ZM-MO1957-292	Iraq-Kirkuk-Kirkuk, Mullaabdolah			A-B-C/10
MNHN ZM-MO1957-193	Iraq-Soleymanie, Penjwin			A-B-C/10
MNHN ZM-MO1957-196	Iraq-Soleymanie, Penjwin			A-B-C/10
MNHN ZM-MO1957-198	Iraq-Soleymanie, Penjwin			A-B-C/10
MNHN ZM-MO1957-200	Iraq-Soleymanie, Penjwin			A-B-C/10
MNHN ZM-MO1957-201	Iraq-Soleymanie, Penjwin			A-B-C/10
MNHN ZM-MO1957-203	Iraq-Soleymanie, Penjwin			A-B-C/10
MNHN ZM-MO1957-204	Iraq-Soleymanie, Penjwin			A-B-C/10
MNHN ZM-MO1957-210	Iraq-Soleymanie, Penjwin			A-B-C/10
MNHN ZM-MO1957-211	Iraq-Soleymanie, Penjwin			A-B-C/10
MNHN ZM-MO1957-214	Iraq-Soleymanie, Penjwin			A-B-C/10
MNHN ZM-MO1957-216	Iraq-Soleymanie, Penjwin			A-B-C/10
MNHN ZM-MO1957-218	Iraq-Soleymanie, Penjwin			A-B-C/10
MNHN ZM-MO1957-222	Iraq-Soleymanie, Penjwin			A-B-C/10
MNHN ZM-MO1957-224	Iraq-Soleymanie, Penjwin			A-B-C/10
MNHN ZM-MO1957-225	Iraq-Soleymanie, Penjwin			A-B-C/10
MNHN ZM-MO1957-226	Iraq-Soleymanie, Penjwin			A-B-C/10
MNHN ZM-MO1957-231	Iraq-Soleymanie, Penjwin			A-B-C/10
MNHN ZM-MO1957-234	Iraq-Soleymanie, Penjwin			A-B-C/10
MNHN ZM-MO1957-238	Iraq-Soleymanie, Penjwin			A-B-C/10
MNHN ZM-MO1957-243	Iraq-Soleymanie, Penjwin			A-B-C/10
MNHN ZM-MO1957-245	Iraq-Soleymanie, Penjwin			A-B-C/10
MNHN ZM-MO1957-247	Iraq-Soleymanie, Penjwin			A-B-C/10
MNHN ZM-MO1957-251	Iraq-Soleymanie, Penjwin			A-B-C/10
MNHN ZM-MO1957-253	Iraq-Soleymanie, Penjwin			A-B-C/10
MNHN ZM-MO1957-258	Iraq-Soleymanie, Penjwin			A-B/10
MNHN ZM-MO1957-264	Iraq-Soleymanie, Penjwin			A-B/10
MNHN ZM-MO1957-265	Iraq-Soleymanie, Penjwin			A-B/10
MNHN ZM-MO1957-268	Iraq-Soleymanie, Penjwin			A-B/10
MNHN ZM-MO1957-273	Iraq-Soleymanie, Penjwin			A-B/10
MNHN ZM-MO1957-275	Iraq-Soleymanie, Penjwin			A-B-C/10
MNHN ZM-MO1960-3872	Iraq-Soleymanie, Penjwin			A-B-C/10

doi: 10.1111/jzs.12145

lineage to determine whether a population expansion occurred in the past and to characterize it (Rogers and Harpending 1992). Excoffier et al. (2005) proposed to use these mismatch distributions to select between two models: a 'pure demographic expansion' and a 'spatial expansion'. Both assume that a stationary haploid population of size N_0 suddenly grew T generations ago to reach a population size of N_1 haploid individuals. However, while the 'pure demographic expansion' model assumes that the growing population is panmictic, the 'spatial expansion' model involves a spatial range expansion and spatially structured populations. To test the fit of these two models to our data, as well as to estimate the scaled expansion time (Tau) and migration rate parameter (M) in the second model, we used the least-square fitting algorithm implemented in ARLEQUIN v 3.11. Model choice and confidence intervals for parameter estimates are based on a parametric bootstrap approach with 1000 bootstrap replicates. Theta 0 is the size of the population before the expansion, and theta 1 is the size of the population after the expansion.

Geometric morphometric analyses

Only adult specimens with fully erupted and worn molars were incorporated into the morphological analyses. The ventral sides of 258 skulls (Fig. 2, Figure S1 and Table 1) were photographed using a Leica Z6 macroscope coupled to a Leica DFC420 six-megapixel digital camera. We retained in our analyses only the ventral view because it includes most of the taxonomically informative structures (tympanic bullae, tooth rows, palatine foramen; Tabatabaei Yazdi and Adriaens 2013). Twenty-five-two-dimensional (2D) landmarks (Figure S1 and Table S1) were digitized on the images using TpsDig 2.17 (Rohlf 2013). These landmarks (combination of landmarks of types I, II and III; Bookstein 1991) were previously used by Tabatabaei Yazdi and Adriaens (2011), Tabatabaei Yazdi et al. (2012) and Tabatabaei Yazdi and Adriaens (2013) and adapted by E. Stoetzel and M. Dianat. To quantify and visualize the repeatability of the landmarks, we measured ten times three specimens of the same sex, same age class, same locality and same genetic clade. Then, a PCA was performed. It showed that intraspecimen shape variability was lower than interspecimen shape variability.

We defined 11 groups based on the range of subspecies according to bibliographical data, genetic results and geographical origin of specimens (Fig. 2): groups 1, 3 and 4 include specimens that come from the geographical range of *M. p. gurganensis*, *M. p. ambrosius* and *M. p. rossicus*, respectively, and for which molecular data are available. Specimens from the geographical range of *M. p. persicus* were split into three groups: those from eastern Iran (group 5, no molecular data available), those from northern Iran (group 6, no molecular data available) and those from central Iran (group 7, corresponding to lineage IIB). Specimens from the geographical range of *M. p. baptistae* were split into two groups: those from south-east Iran, in the eastern mountains (group 2, corresponding to lineage IIA), and those from the Kerman Province, south-east of the Kohrud Mountains (group 8, no molecular data available). No subspecies name is available in the literature for the specimens captured in the geographical regions corresponding to our groups 9, 10 and 11. These three groups were based on geographical origin (group 9 = south of the Zagros Mountains and genetically corresponds to lineage IB, group 10 = Iraq with no molecular data, group 11 = north-west of Iran and genetically corresponds to lineage IA).

We follow the classical GM approach (Zelditch et al. 2012): (I) we extracted the centroid size of each skull (the square root of the summed squared distances of each landmark to the centroid) and (II) we performed three general Procrustes superimpositions to extract shape variables (Rohlf and Slice 1990): (A) with all specimens (n = 258), (B) without groups 3 and 9 (n = 254) that possess only two specimens each, and one (C) with only sexed specimens (n = 188). For the three data sets, we performed a principal components analysis (PCA) on shape variables to reduce the dimensionality, and kept the first axe, which accounts for 90% of the shape variability.

To test the statistical differences in size and shape between groups in data set B, we performed an analysis of variance (ANOVA) on log-transformed (normalization) centroid sizes and a multiple analysis of variance (MANOVA) on shape variables, respectively. Then, we performed a linear discriminant analysis (LDA) on shape variables in data set B to quantify and show shape differences between groups. Finally, to highlight the overall shape differences between groups, a neighbor-joining tree (NJ) based on Mahalanobis distances was performed on all shape variables.

To avoid the problems linked with the few number of specimens in groups 3 and 9 (Evin et al. 2012), we used an alternative approach to LDA on data set A: the K nearest neighbor (KNN) (Ripley 1996). This method is less sensitive to small sample size (Baylac and Frieß 2005) and has been used for group discrimination (Cornette et al. 2015). A specimen is assigned to the most common group among its K nearest neighbors using Euclidian distances. Here, we used k = 4, which has given the best results of group classification after testing from k = 1 to k = 5. The results of the best classification allowed us to calculate a discrimination level between the groups.

To test for sexual dimorphism, we performed an ANOVA on log-transformed centroid size and a MANOVA on shape in data set C.

All statistical analyses were performed using R (R Core Team 2014), using the libraries 'R-morph' (Baylac 2012) for generalized Procrustes analysis and PCA, 'MASS' for LDA, 'class' for KNN calculation (Venables and Ripley 2002) and 'ape' for NJ (Paradis et al. 2004).

To estimate the phylogenetic signal in skull shape, we used a randomization test following the method of Blomberg et al. (2003). A multivariate K-statistic (Adams 2014) was calculated based on the Procrustes coordinates using the 'geomorph' library (Adams and Otarola-Castillo 2013) in R (R Core Team 2014).

This statistic indicates whether the shape variation is as structured by phylogeny as expected under Brownian motion model of evolution (Kmult = 1) or shows higher (Kmult > 1) or lower (Kmult < 1) phylogenetic signal.

Species distribution modelling

We modelled the climatic niche of *M. persicus* to approximate its current and last glacial maximum (LGM) distribution. We applied ecological niche modelling methods, where environmental data are extracted from current occurrence records and habitat suitability is evaluated across the landscape using program-specific algorithms (Elith et al. 2006). The present-day models were then projected on the climatic reconstructions of the LGM under the assumption that the climatic niche of each species remained conserved between the LGM and present (Elith et al. 2010).

The occurrences were derived from the online database Global Biodiversity Information Facility (http://www.gbif.org, Last access date: 26 October 2015), from the specimens included in our molecular or morphometric analyses and from the literature, including Hatt (1959), Roberts (1977), Habibi (1977), Krystufek and Vohralik (2009) and Etemad (1978). To correct for sampling bias, a subsample of records regularly distributed in the geographical space was selected using the stand-alone program ENMTools v 1.3 (Warren et al. 2010), with a grid reference of 2.5 arc minutes (~5 × 5 km). This method is efficient in correcting for sampling bias (Fourcade et al. 2014). Finally, 173 presence records were used for the species distribution modelling.

A set of 19 bioclimatic variables were downloaded from the WorldClim database (Hijmans et al. 2005), at a spatial resolution of 2.5′, to be used as environmental predictors that comprehensively describe the climatic conditions of the study area. This coarser resolution was chosen over the available 30 arc second data to better match the coordinate uncertainties associated with georeferenced, textual localities of museum specimens. We remove highly correlated variables (i.e. with a Pearson's correlation coefficients > 0.75), resulting in the selection of seven predictor variables (BIO 1: Annual Mean Temperature; BIO 2: Mean Diurnal Range; BIO 7: Temperature Annual Range; BIO 12: Annual Precipitation; BIO 14: Precipitation of Driest Month; BIO 15: Precipitation Seasonality; BIO 19: Precipitation of Coldest Quarter).

Climatic variables were used for present conditions and for the LGM. LGM climate data were drawn from the general circulation model (GCM) simulations based on two climate models: the Community Climate System Model (CCSM, version 3) (Collins et al. 2006) and the Model for Interdisciplinary Research on Climate (MIROC, version 3.2) (Hasumi and Emori 2004). These climate models differ in temperature and precipitation patterns. LGM climate as simulated by CCSM3 is colder and dryer than that of MIROC. For a discussion of the uncertainties associated with the climatic data, see Schorr et al. (2012) and Varela et al. (2015). The use of these two different climate models enabled us to assess and account for modelling the uncertainty due to LGM climate data. To predict the potential distribution of the species in current conditions and in the LGM, we used Maxent v 3.3.3 (Phillips et al. 2006), which outputs a model with relative occurrence probability of a species

doi: 10.1111/jzs.12145

within the grid cells of the study area. To ensure the consistency of model predictions among repeated runs, we performed a 50-fold cross-validation with random seeds. To determine whether the predictions for current conditions generated by Maxent were better than random predictions, we used the area under the receiver-operating characteristic curve (AUC), a commonly used measurement for comparison of model performance (Elith et al. 2006). The AUC score varies from 0 to 1, with greater scores indicating better discrimination ability; an AUC score greater than 0.5 indicates that the model discriminates better than random (Phillips and Dudik 2008).

Results

Phylogenetic results

No indels or stop codons were observed, suggesting that no nuclear copies of mtDNA were present in the data set. The species *Meriones persicus* forms a monophyletic group (posterior probability (PP) = 1; Fig. 3).

Results of the phylogenetic and network analyses are congruent (Figs 3 and 4) and highlight the existence of several lineages within *M. persicus*, with a strong phylogeographical structure. Two main lineages, I and II, can be identified (PP = 1 for both; Fig. 3). Lineage I is composed of specimens from western part of Iran (in Fig. 5: black circles), from Zagros Mountains and western Alborz Mountains. Within lineage I, the two specimens from Baghe Shadi (lineage IB; refer to Fig. 5: 1) cluster together and are genetically divergent from other specimens. Lineage II is composed of all specimens from the eastern mountains of Iran, Kohrud Mountains and southern Zagros Mountains. Within lineage II, two sublineages (IIA and IIB) can be identified (PP = 1 and 0.99, respectively). Lineage IIA is composed of specimens from Kopet Dagh, eastern part of Alborz Mountains and eastern mountains (in Fig. 5: blue circles). Lineage IIB is composed of specimens from Kohrud Mountains and southern Zagros Mountains (in Fig. 5: red circles).

In the network (Fig. 4), there is some discrimination within lineage IIA between specimens of the two subspecies *M. p. baptistae* and *M. p. gurganensis*. They both form a monophyletic group, except for two specimens of *M. p. gurganensis* (haplotype 26) coming from Neyshabour, Soomee (Locality 17) that do not cluster together. The two specimens of *M. p. ambrosius* share the same haplotype (haplotype 49). Three specimens from Dare Gahan (Yazd Province, Taft; haplotypes 9 and 10, Locality 35) are genetically divergent (nine mutations) from all other specimens of *M. p. persicus*.

Genetic divergence and diversity

The mean percentage of sequences divergence (K2P) between lineages for *cyt b* ranges from 2.5% (between lineages IIA and

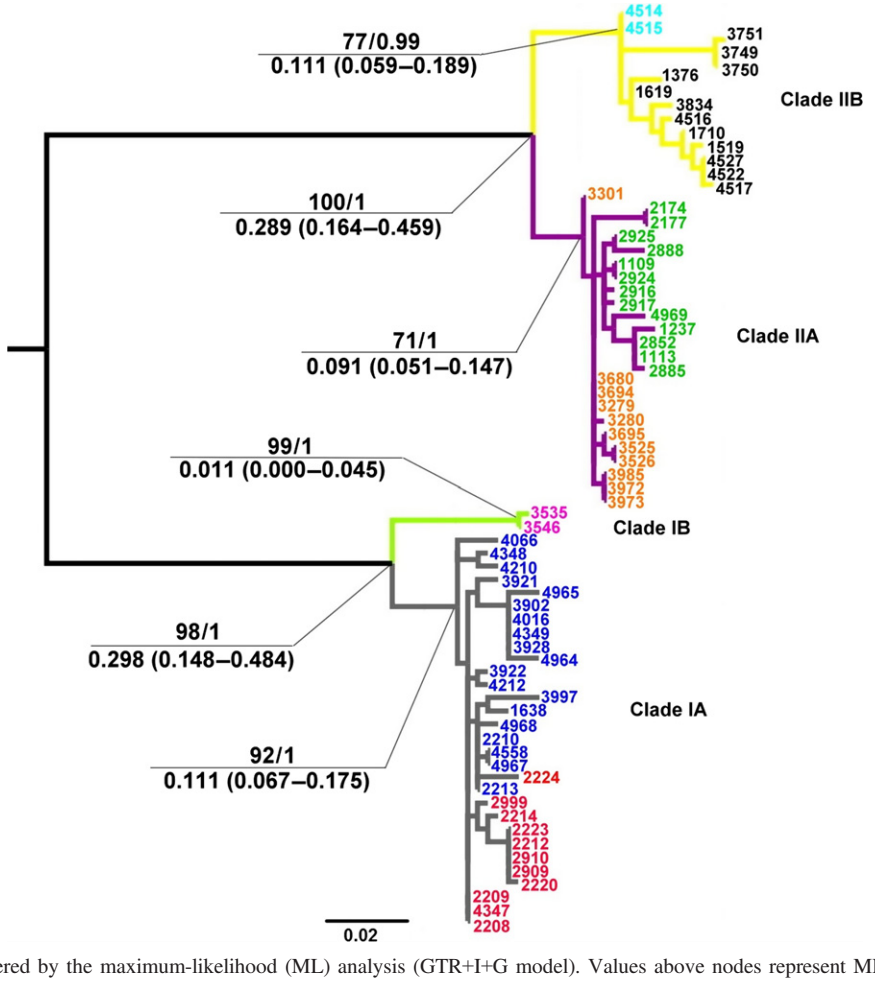

Fig. 3. Phylogeny recovered by the maximum-likelihood (ML) analysis (GTR+I+G model). Values above nodes represent ML bootstrap supports and Bayesian posterior probabilities derived from the maximum clade credibility chronogram derived from an analysis in BEAST and a relaxed clock, respectively. Values below nodes indicate divergence time estimates with the highest posterior density (HPD) interval containing 95% of the sampled values within brackets. The numbers in red correspond to *M. p. rossicus*; black: *M. p. persicus*; green: *M. p. gurganensis*; orange: *M. p. baptistae*; light blue: *M. p. ambrosius*; blue: no report 1; and light violet: no report 2 (based on bibliographical data). Lineage IA: grey; Lineage IB: light green; Lineage IIA: violet; Lineage IIB: yellow

doi: 10.1111/jzs.12145

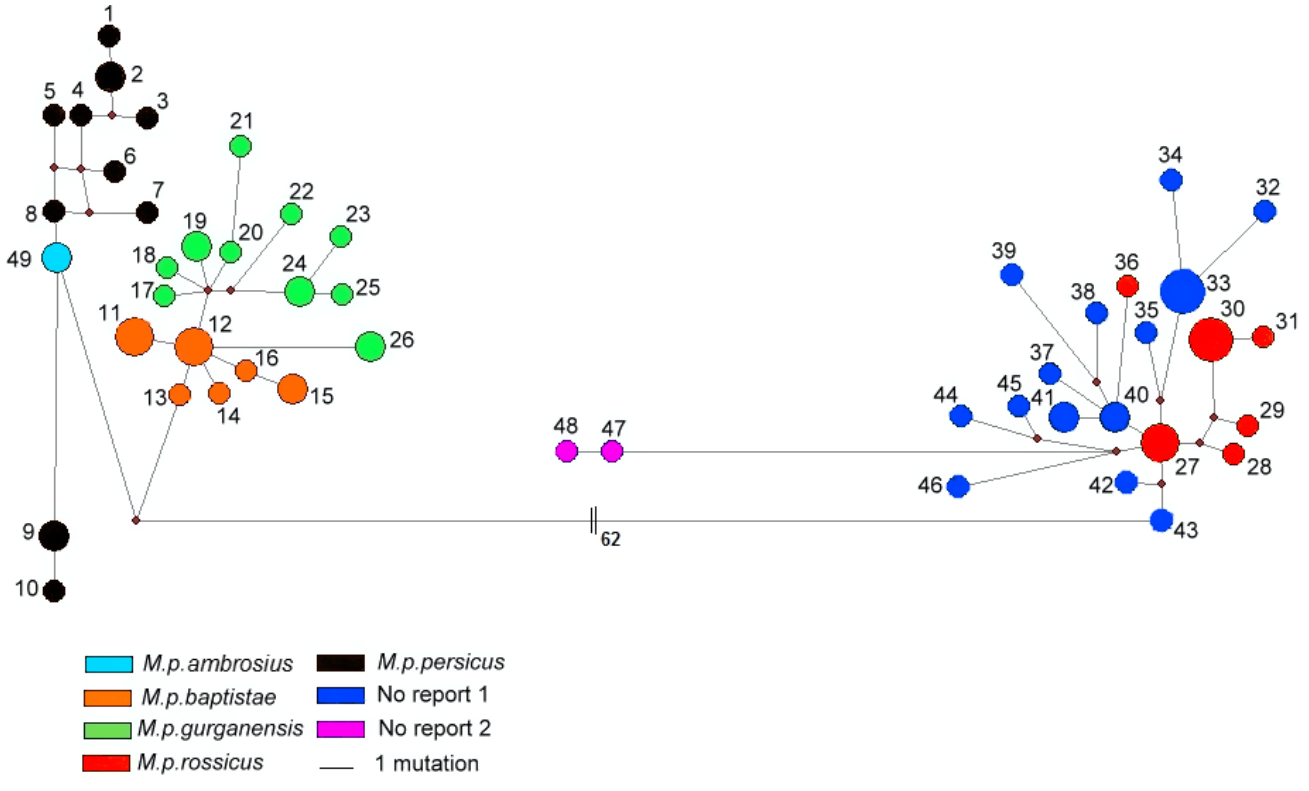

Fig. 4. Median-joining network obtained for the *cyt b* gene. Circle sizes are proportional to the number of the same haplotypes observed in the data set. Branch lengths are proportional to the number of mutations between haplotypes, except when the symbol || is indicated. The number below this symbol indicates the number of mutations between haplotypes. Other numbers indicate haplotype numbers (see Table 1). Colours indicate subspecies according to bibliographical data: Red: *M. p. rossicus*; black: *M. p. persicus*; green: *M. p. gurganensis*; orange: *M. p. baptistae*; light blue: *M. p. ambrosius*; blue and light violet: no available subspecies name from north (no report 1) and south (no report 2) Zagros Mountains, respectively. Missing haplotypes are represented by very small red circles.

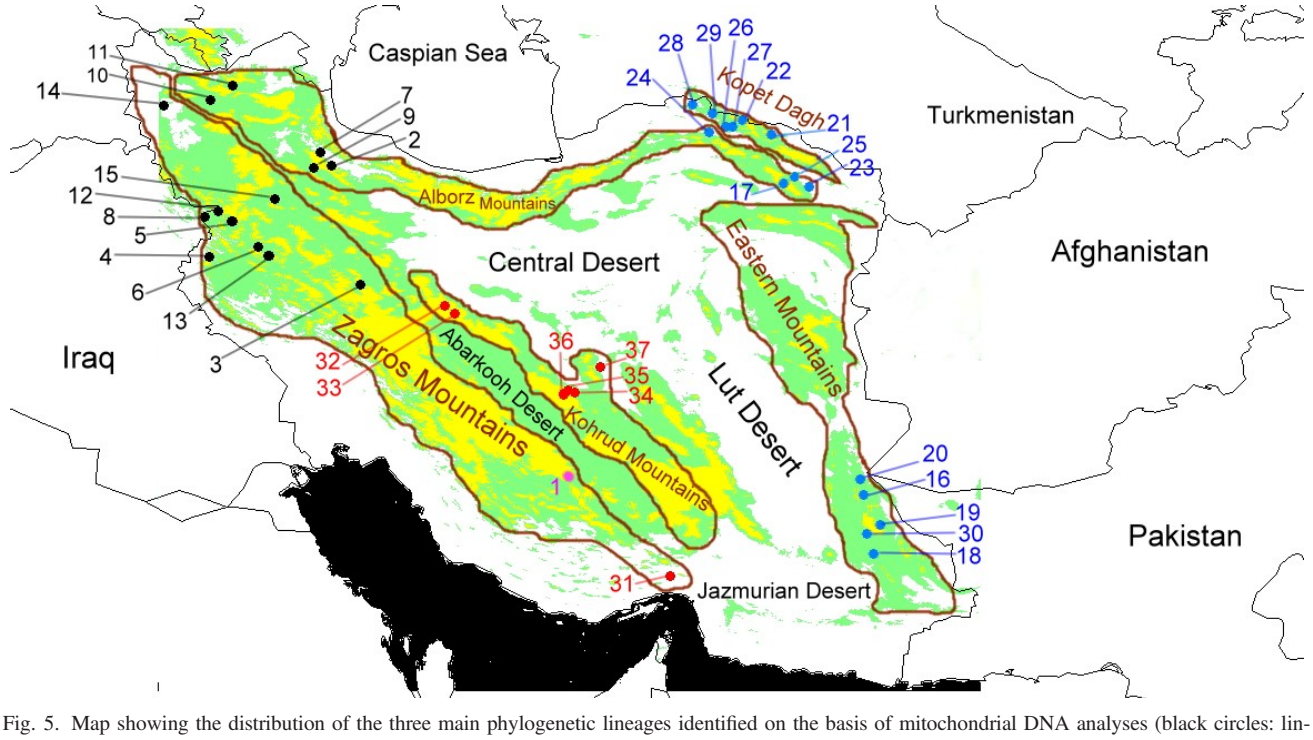

Fig. 5. Map showing the distribution of the three main phylogenetic lineages identified on the basis of mitochondrial DNA analyses (black circles: lineage IA; pink circle: lineage IB; red circles: lineage IIB; blue circles: lineage IIA). Borders and names of mountains are in brown. Name of deserts mentioned in the text are in black. Numbers indicate the localities of collect (see Table 1). Colours indicate altitude: white: altitude below 1270 m; green: altitude between 1270 and 2000 m; yellow: altitude higher than 2000 m

doi: 10.1111/jzs.12145

IIB and between IA and IB) to 9.6% (between lineages IA and IIB). Within lineages, the mean percentages of sequence divergence ranges from 0.1 (lineage IB) to 0.9 (lineage IIB) (Table 2). The genetic distance between the two specimens from Baghe Shadi (refer to Fig. 5: Locality 1) and other specimens of lineage I is 2.5%.

Haplotype diversity is high in all lineages (0.961 ± 0.020–1.000 ± 0.500; Table 3). Nucleotide diversity and the mean number of differences are highest in lineage IIB and lowest in lineages IB and IIA.

We tested for signatures of population expansion in lineages IA, IIA and IIB. A significant signal of population expansion was obtained in lineage IA for Fu's Fs and Tajima D tests. A significant signal of population expansion was obtained in lineage IIA for the Fu's Fs test, and it was nearly significant (p = 0.056) for the Tajima's D test. Based on mismatch analyses, a significant signal of demographic and spatial expansion was recorded in the three lineages (p > 0.05; Fig. 6). According to theta 0 and theta 1 values, the intensity of the demographic expansion was similar between clades (Table 3). Tau values did not differ significantly between lineages, suggesting that population expansions occurred simultaneously in the three lineages (Table 3).

Divergence time estimates

The time to the most recent common ancestor (TMRCA) of the *M. persicus* complex is estimated to be 1.439 Mya (highest posterior density (HPD) interval containing 95% of the sampled values: 0.888–2.124). The TMRCAs for lineages I and II are estimated to be 0.298 [0.148–0.484] and 0.289 [0.164–0.459] Mya, respectively. The TMRCAs of lineages IIA and IIB are estimated to be 0.091 [0.051–0.147] and 0.111 [0.059–0.189] Mya, respectively (Fig. 3).

Table 2. The K2P divergences between and within (Bold numbers) lineages of *Meriones persicus* for *cyt b* gene

clusD				
knnD	Lineage IA	Lineage IB	Lineage IIA	Lineage IIB
Lineage IA	**0.7**			
Lineage IB	2.5	**0.1**		
Lineage IIA	8.9	9.4	**0.5**	
Lineage IIB	9.6	9.7	2.5	**0.9**

Geometric morphometrics

There is no significant difference in size between the groups (p = 0.745). There is a significant difference in shape between

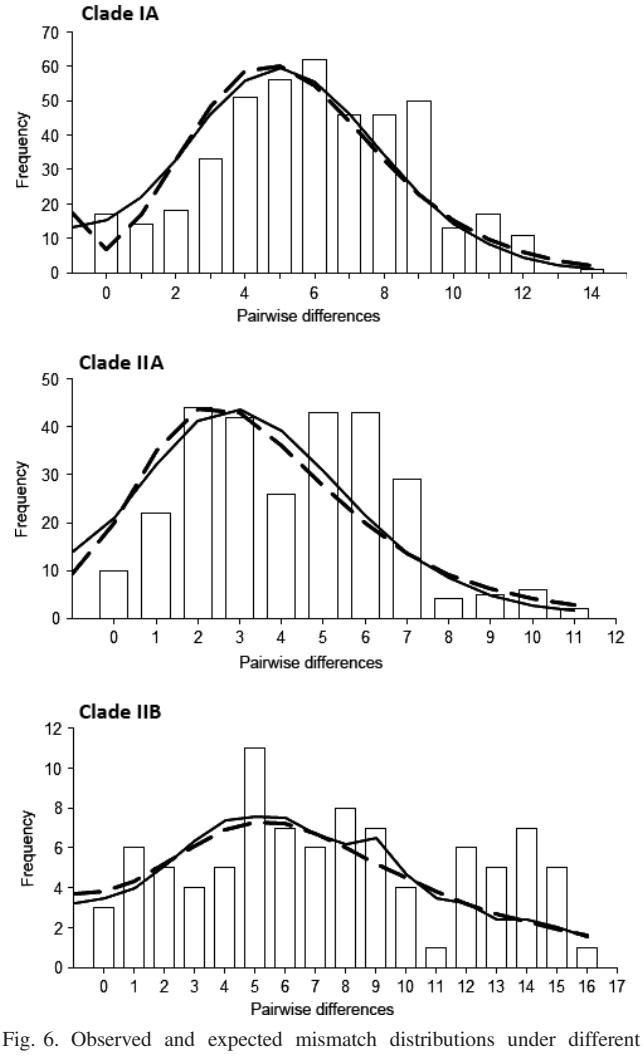

Fig. 6. Observed and expected mismatch distributions under different models. White bars, observed distributions; solid lines, pure demographic expansion in an unsubdivided population model; dashed lines, range expansion in the infinite-island model

Table 3. Diversity and neutrality estimates and results of the mismatch analyses for the main lineages of *Meriones persicus* identified in the phylogenetic analyses. N, the number of specimens; Np, the number of polymorphic sites; Nh, the number of haplotypes; Hd, haplotype diversity; Pi, nucleotide diversity; k, average number of nucleotide differences; Tau, scaled expansion time; theta 0, size of the population before the expansion; theta 1, size of the population after the expansion. For tau, theta 0 and theta 1, estimated values and ranges (p value of 0.05) are given. For Fu's Fs and Tajima's D tests, the symbol '*' indicates significant values.

	IA	IB	IIA	IIB
N	30	2	24	14
Np	43	1	27	22
Nh	20	2	16	11
Hd	0.961 ± 0.020	1.000 ± 0.500	0.964 ± 0.022	0.967 ± 0.037
Pi	0.00684 ± 0.01238	0.00114 ± 0.00057	0.00493 ± 0.00064	0.00866 ± 0.00110
k	5.995	1.000	4.324	7.593
Fu's Fs	−7.938*		−7.345*	−2.286
Tajima's D	−1.656*		−1.543	0.411
Tau	6.1 (3.3–11.1)		3.7 (1.4–9.3)	5.1 (1.9–16.7)
Theta 0	0.6 (0–3)		1 (0–4)	5 (0–13)
Theta 1	33 (15–99 999)		23 (11–99 999)	24 (12–99 999)
M	24 (12–142)		76 (12–99 999)	15 (1–99 999)

doi: 10.1111/jzs.12145

the groups ($p < 2.2e-16$). There is sexual dimorphism in size ($p = 0.00976$), but no differences in shape ($p = 0.2346$). The LDA (Fig. 7) and NJ tree (Fig. 8) both indicate that groups 4, 6, 10 and 11 have similar ventral skull shape. These groups are morphologically highly similar and the percentage of correct classification within these groups is low (from 0% in group 4 to 77% in group 10; Table S2). When these four groups are considered together, the percentage of correct classification within this group is very high (97–100%). These four groups can be differentiated from other groups by their proportionally smaller tympanic bulla, longer rostrum and more curvated zygomatic arch. In the LDA and NJ tree, groups 1, 2, 5, 7 and 8 tend to cluster together, but with some variability in ventral skull shape between them. Group 1 is the most morphologically different (82% of correct classification). It can be differentiated from groups 4-6-10-11 and 2-5-7-8 by its intermediate position on the first axis (i.e. tympanic bulla and rostrum length of intermediate shape and zygomatic arch of intermediate position) and by a slightly different position on the second axis of the LDA (most anterior point of the zygomatic process concavity formed by the temporal bone situated more posteriorly on the skull than in other groups; Figs 7 and 9). The percentage of correct classification is 42%, 75%, 77% and 62% for groups 5, 8, 10 and 11, respectively. The percentage of correct classification is very low for group 2 (27%), and this group is morphologically close to groups 1, 7 and 8 (36–18% of individuals of group 2 classified in these groups).

The multivariate measure of phylogenetic signal was estimated as Kmult = 0.036, below the Brownian expectation of 1, but significantly greater than expected if traits were unstructured by phylogeny ($p < 0.001$).

Species distribution modelling

To study the relationships between genetic diversity and possible glacial refugia, we built a species distribution model (Fig. 10) for *M. persicus* based on the known-presence localities of this species. The AUC value was 0.989, which is considered to correspond to a useful predictive model. The model revealed high habitat suitability for this species across most Iran (except desert and coastal zones) under present-day climatic conditions, in agreement with the current known distribution of the species (Fig. 10). The MIROC predicted very mild climatic conditions for the LGM in this part of the world, and thus, the distribution predicted for *M. persicus* in the LGM is very similar to the present distribution, except lower habitat suitability in the eastern mountains. According to the CCSM, the suitable habitat for *M. persicus* during the LGM was patchily distributed in the north-western Zagros Mountains (including Iraq), north-eastern Alborz Mountains, central Zagros (area of Baghe Shadi) and Kohrud Mountains, and south-eastern Iran.

Discussion

Taxonomy

Our *cyt b* genetic data emphasize high genetic variability within *M. persicus* in Iran: the mean percentage of sequences

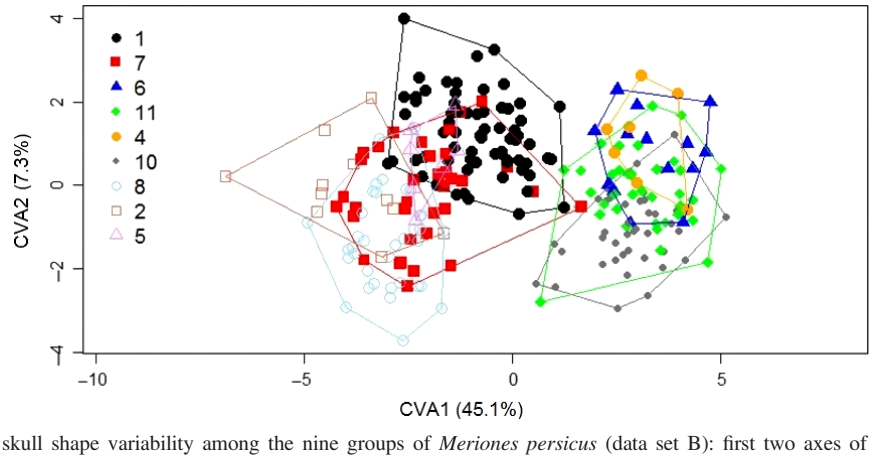

Fig. 7. Ventral view of skull shape variability among the nine groups of *Meriones persicus* (data set B): first two axes of the discriminant analyses (45.1% and 7.3% of total variance, respectively)

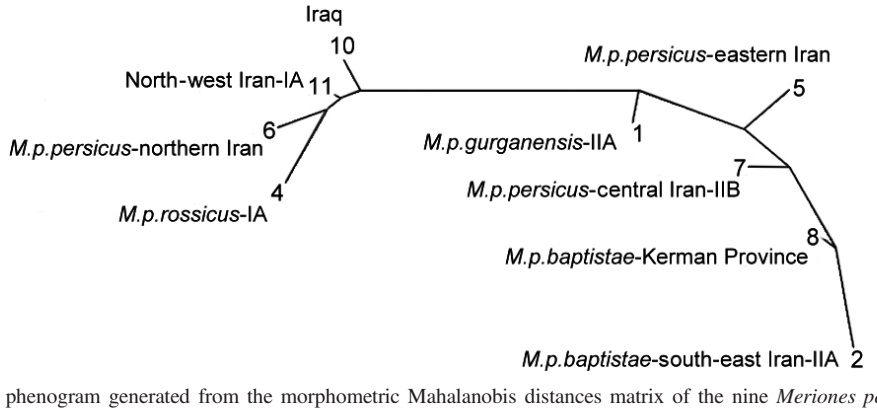

Fig. 8. Neighbor-joining phenogram generated from the morphometric Mahalanobis distances matrix of the nine *Meriones persicus* groups. Numbers indicate the nine morphometric groups included in data set B (see material and methods section: groups 1, 2, 4 to 8, 10 and 11). Geographical origin and subspecies are provided for each group, except groups 10 and 11 for which no subspecies names are available in the literature for these geographical regions

doi: 10.1111/jzs.12145

divergence (K2P) between lineages ranges from 2.5% to 9.6%. Using mtDNA genetic distances only to infer the specific status of taxa may be misleading (e.g. Bradley and Baker 2001), but the comparison with the published studies can give interesting results. The value of 9.6% is high and more often corresponds to interspecific variation in rodents, but it can also sometimes be observed within species, while the value of 2.5% is commonly observed within species, and particularly between subspecies of a given species, and sometimes between sister species (Bradley and Baker 2001; Nicolas et al. 2012). Observed genetic distances within *M. persicus* in Iran favour the hypothesis that several subspecies could be defined within.

According to the literature, five subspecies with allopatric geographical distributions were reported in Iran (Fig. 1). These subspecies were defined mainly based on external (e.g. fur colour) and skull diagnostic features. However, Tabatabaei Yazdi and Adriaens (2011) showed only smooth variation in cranial characters between subspecies; the shape of the skull was correlated with geoclimatic factors: Persian jirds from the southern populations living in lower, warmer and drier localities are characterized by bulla hypertrophy, less convex zygomatic arch, narrower zygomatic plate, longer incisive foramen and a slightly shorter nasal. Our molecular data highlight the existence of four genetic lineages in Iran, but they only partly correspond to these subspecies. The result of multivariate *K*-statistic indicates that phylogeny significantly influences the skull shape variation, but that closely related genetic lineages resemble each other phenotypically less than expected under Brownian motion. This result suggests that other factors than phylogeny, like ecology and/or bioclimatic factors, may influence *M. persicus* skull morphology, as already suggested by Tabatabaei Yazdi and Adriaens (2011).

Lineage IA groups together all specimens north of the Zagros Mountains and north-west of the Alborz Mountains. Our morphometric analyses also show that all specimens of lineage IA are morphologically very close (groups 4 and 11) and are also very close to those found in Iraq (group 10) and the western part of Alborz Mountains (group 6). This result is congruent with those obtained by Tabatabaei Yazdi and Adriaens (2011). Lineage IA could correspond to the subspecies *M. p. rossicus,* which ranged from Turkey to Armenia and probably in the north-west of Iran (Ellerman and Morrison-Scott 1951; Krystufek and Vohralik 2009; Boudet 2010; Darvish et al. 2014). If this is true, it would suggest that the geographical range of this subspecies should be extended southward, up to Namak Koor, Arak in Markazi Province and eastward to Tehran Province.

According to Neuhausee (1936), *M. p. rossicus* is characterized by elongated rostra and nasal bones and a relatively small crania. Its zygomatic arch is relatively narrow, and the tympanic bulla is not very large. The front wall of the auditory meatus forms a large laterally directed projection. Our geometric morphometric results suggest that groups 6-4-10 and 11 could correspond to *M. p. rossicus* owing to their elongated rostrum and small tympanic bulla.

Lineage IIA is composed of specimens from eastern Iran: Kopet Dagh, eastern part of the Alborz Mountains and the eastern mountains. Based on its geographical origin, this lineage could correspond to two subspecies: *M. p. gurganensis* in the north and *M. p. baptistae* in the south. Our network analysis indicates some genetic differentiation between these subspecies, but with overlap. Our analyses show that specimens that belong geographically to *M. p. gurganensis* form a distinct morphologic entity (group 1), characterized by a tympanic bulla and rostrum length of intermediate size and a zygomatic arch of intermediate position. In this group, the most anterior point of the zygomatic process concavity formed by the temporal bone tends to be situated more posteriorly on the skull than in other groups. These characters only partly fit those used to describe *M. p. gurganensis*, which, compared to *M. p. persicus*, has a long and narrow skull, slender rostrum, long and narrow nasals and large bullae,

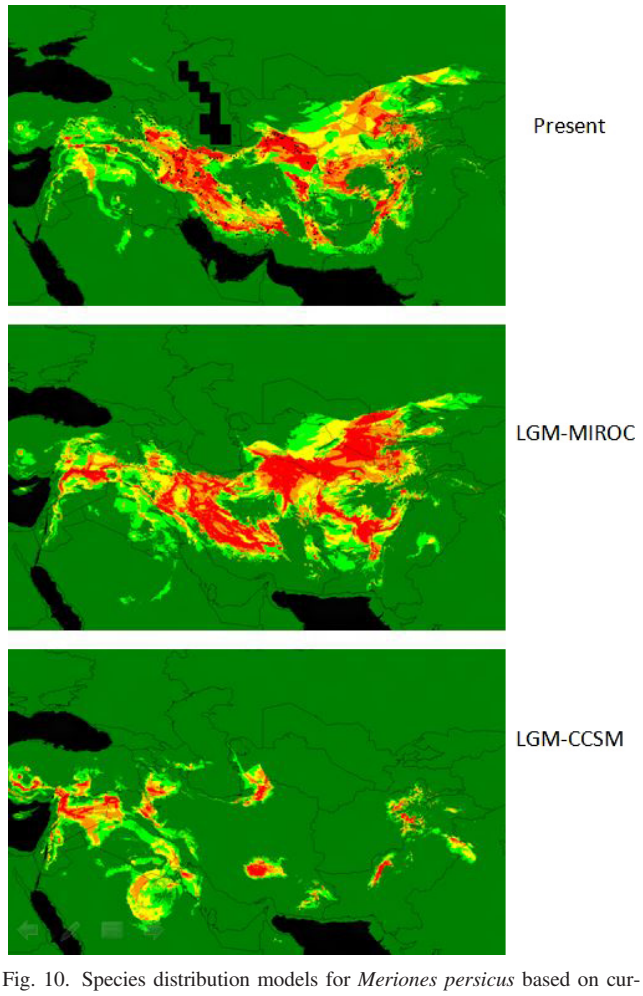

Fig. 10. Species distribution models for *Meriones persicus* based on current distribution and projection of this model to the last glacial maximum (LGM) based on two palaeo-climatic models: the Model for Interdisciplinary Research on Climate (MIROC) and the Community Climate System Model (CCSM). Warmer colours show areas with higher probability of presence. Black plots on the first map indicate the known-presence records for this species.

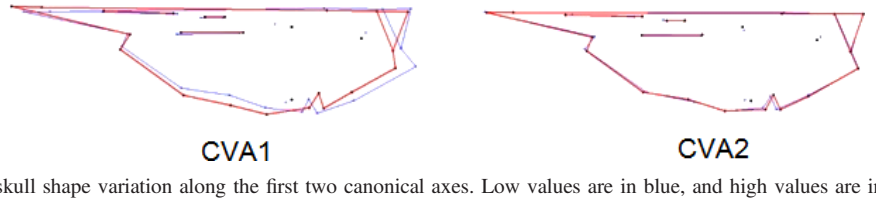

Fig. 9. Visualization of skull shape variation along the first two canonical axes. Low values are in blue, and high values are in red.

doi: 10.1111/jzs.12145

extending posteriorly beyond the occipital condyles (Goodwin 1939).

Specimens belonging geographically to *M. p. baptistae* (groups 2 and 8) do not form a well-defined morphological group. According to Thomas (1920), the skull of this subspecies is very similar to those of *M. p. persicus*, except that the bullae are larger, more fully inflated and generally project backwards behind the level of the back of the supraoccipital. In *M. p. persicus*, they fall decidedly short of the same level (Thomas 1920). The validity of the subspecies *M. p. baptistae* is doubtful and requires additional molecular and morphological data to be tested further.

Lineage IIB is composed of specimens from the Kohrud Mountains and southern Zagros Mountains. Based on its geographical origin, this lineage could correspond to two subspecies: *M. p. ambrosius* and *M. p. persicus*. Only few specimens of *M. p. ambrosius* could be included in our molecular and morphometric analyses, and our preliminary results do not allow us to validate this subspecies. Additional analyses with more specimens are needed to conclude definitively. *Meriones p. persicus* was described based on its narrower nasal and the different shape of its zygomatic arch and foramen magnum zone (Blanford 1876).

Our molecular analyses highlighted the existence of a distinct lineage (lineage IB) south of the Zagros Mountains. No subspecies name is available for this part of the country. It would be interesting to add more specimens in molecular and morphometric analyses to further test the distinctiveness of this population.

Finally, it is necessary to include in our molecular analyses specimens from groups 5 and 8 to test whether they are more closely related to lineage IIA or IIB.

Phylogeography

The separation of the different entities in Iran seems to fit the geomorphology of the country: the Abarkooh Desert separates lineages I (Zagros Mountains and west of Alborz Mountains) and IIB (Kohrud Mountains and southern Zagros Mountains), while the Central Desert and Lut Desert separate lineages IIB (Kohrud Mountains and southern Zagros Mountains) and IIA (eastern mountains, eastern Alborz Mountains and Kopet Dagh Mountains). The role of the Central and Lut deserts as geographical barriers between Zagros or Kohrud Mountains populations and Kopet Dagh or eastern Alborz populations was previously emphasized in several phylogeographical studies (Stöck et al. 2006; Dubey et al. 2007; Rajaei et al. 2013; Shahabi et al. 2013; Haddadian-Shad et al. 2016). No genetic differentiation was found between Zagros Mountains and Kohrud Mountains (locality of Kerman) populations of green toad (Stöck et al. 2006) and brush-tailed mice (Shahabi et al. 2013). White-toothed shrew populations from central Iran (Kerman and Esfahan) are genetically divergent from populations from the north-west, but the origin of this differentiation was not investigated (Dubey et al. 2007).

Our divergence time estimates show that all intraspecific divergent events within the Persian Jird occurred during the last 1.4 My. The Quaternary Period was dominated by Ice Ages and involved repeated global cooling and increasing of the Arctic and Antarctic ice sheets (Hewitt 2004). According to our divergence time estimates, it seems likely that the populations of *M. persicus* started to diverge during earlier phases of the glacial periods and not during the last glaciation. In the absence of available climatic data for previous glacial periods, we used the LGM conditions as a proxy of the palaeo-climatic conditions of glacial periods. However, it should be stressed that the intensity of glaciations was not always the same from one glacial cycle to another and that even for the LGM several uncertainties are associated with the climate data. One major point is the reliability of global circulation models for the LGM climate (Schorr et al. 2012). In our data, uncertainty resulting from climate model is evident from the LGM species distributions obtained with the CCSM and MIROC. The MIROC predicted very mild climatic conditions for the LGM in this part of the world (Schorr et al. 2012), and thus, the distribution predicted for *M. persicus* in the LGM is very similar to the present distribution, except lower habitat suitability in the eastern mountains. Thus, the results of the MIROC do not explain the deep genetic divergence observed between *M. persicus* populations from Zagros Mountains (lineage I) and Kohrud Mountains (lineage IIB). According to the CCSM, the suitable habitat for *M. persicus* during the LGM was patchily distributed in the north-western Zagros Mountains (including Iraq), north-eastern Alborz Mountains, central Zagros (area of Baghe Shadi), Kohrud Mountains, and south-eastern Iran. Results of the CCSM are congruent with our *cyt b* phylogenetic tree and suggest that potential refugial areas persisted during glacial periods for this species in north-western Zagros Mountains (lineage IA), north-eastern Alborz Mountains (lineage IIA) and Kohrud Mountains (lineage IIB). Moreover, our mismatch analyses show that a demographic and spatial expansion occurred simultaneously in these three lineages. This population expansion was also confirmed by neutrality tests for lineages IA and IIA. These results reinforce the idea that north-western Zagros Mountains, north-eastern Alborz Mountains and Kohrud Mountains could have served as refugia during glacial periods and as source populations for the detected postglacial expansion events.

Acknowledgements

Field work and molecular analyses were supported by Project No. 30812 in Ferdowsi University of Mashhad in Iran. Morphometric analyses were performed at the UMS MNHN/CNRS2700 'Outils et méthodes de la Systématique intégrative'. We are grateful to E. Stoetzel for her help in defining landmarks.

References

Adams DC (2014) A generalized K statistic for estimating phylogenetic signal from shape and other high dimensional multivariate data. Syst Biol **63**:685–697.

Adams DC, Otarola-Castillo E (2013) Geomorph: an R package for the collection and analysis of geometric morphometric shape data. Meth Ecol Evol **4**:393–399.

Adams DC, Slice DE, Rohlf FJ (2004) Geometric morphometrics: ten years of progress following the 'revolution'. Ital J Zool **71**:5–16.

Agard P, Omrani J, Jolivet L, Mouthereau F (2005) Convergence history across Zagros, Iran; constraints from collisional and earlier deformation. Int J Earth Sci **94**:401–419.

Akaike H (1973) Information theory as an extension of the maximum likelihood principle. In: Petrov BN, Csaki F (eds), Second International Symposium on Information Theory. AkademiaiKiado, Budapest, pp 267–281.

Alhajeri BH, Hunt OJ, Steppan SJ (2015) Molecular systematics of gerbils and deomyines (Rodentia: Gerbillinae, Deomyinae) and a test of desert adaptation in the tympanic bulla. J Zool Syst Evol Res **53**:312–330.

Aliabadian M, Kaboli M, Prodon R, Nijman V, Vences M (2007) Phylogeny of Palearctic wheatears (genus *Oenanthe*) congruence between morphometric and molecular data. Mol Phylogenet Evol **42**:665–675.

Bandelt HJ, Forster P, Rohl A (1999) Median-joining networks for inferring intraspecific phylogenies. Mol Biol Evol **16**:37–48.

Barciova L, Macholan M (2006) Morphometric study of two species of wood mice *Apodemus sylvaticus* and *A. flavicollis* (Rodentia:Muridae):

doi: 10.1111/jzs.12145

traditional and geometric morphometric approach. Acta Theriol **51**:15–27.

Baylac M (2012) Rmorph: a R geometric and multivariate morphometrics library. Available from the author: baylac@mnhn.fr.

Baylac M, Frieß M (2005) Fourier descriptors, Procrustes superimposition, and data dimensionality: an example of cranial shape analysis in modern human populations. In: Slice DE (ed), Modern Morphometrics in Physical Anthropology. Springer, US, pp 145–165.

Blanford WT (1876) Eastern Persia. An Account of the Journey of the Persian Boundary Commission 1870-71-72. Vol. **II**. The Zoology and Geology. Macmillan and Co, London.

Blomberg SP, Garland T Jr, Ives AR (2003) Testing for phylogenetic signal in comparative data: behavioural traits are more labile. Evolution **57**:717–745.

Bookstein FL (1991) Morphometric Tools for Landmark Data: Geometry and Biology. Cambridge U Press, Cambridge, UK, pp 1–435.

Boudet Ch (2010) Species Sheet: *Meriones persicus*. Mammals' Planet: Vs n°4, 04/2010. Retrieved May 2015. Available at: http://www.planet-mammiferes.org/drupal/en/node/36?input=meriones+persicus.

Bradley RD, Baker A (2001) A test of the genetic species concept: cytochrome-b sequences and mammals. J Mammal **82**:960–973.

Brown RE (1980) Rodents of the Kavir National Park, Iran. Mammalia **58**:591–600.

Bruford MW, Hanotte O, Brokfield JFY, Burke T (1992) Single-locus and multilocus DNA fingerprinting. In: Hoelzel AR (ed.) Molecular Genetic Analysis of Populations: A Practical Approach. Oxford University Press, New York. pp 225–269.

Cardini A, Elton S (2009) The radiation of red colobus monkeys (Primates, Colobinae): morphological evolution in a clade of endangered African primates. Zool J Linn Soc Lond **157**:197–224.

Cardini A, Jansson AU, Elton S (2007) Ecomorphology of vervet monkeys: a geometric morphometric approach to the study of clinical variation. J Biogeogr **34**:1663–1678.

Castresana J (2001) Cytochrome b phylogeny and the taxonomy of great apes and mammals. Mol Biol Evol **18**:465–471.

Chevret P, Veyrunes F, Britton-Davidian J (2005) Molecular phylogeny of the genus *Mus* (Rodentia: Muridae) based on mitochondrial and nuclear data. Biol J Linn Soc **84**:417–427.

Collins WD, Bitz CM, Blackmon ML, Bonan GB, Bretherton CS, Carton JA, Chang P, Doney SC, Hack JJ, Henderson TB, Kiehl JT, Large WG, McKenna DS, Santer BD, Smith RD (2006) The community climate system model version 3 (CCSM3). J Clim **19**:2122–2143.

Corbet GB (1978) The Mammals of the Palaearctic Region: A Taxonomic Review. Brit Mus Nat Hist. Cornell Univ. Press, London, pp 125–126.

Cornette R, Herrel A, Stoetzel E, Moulin S, Hutterer R, Denys C, Baylac M (2015) Specific information levels in relation to fragmentation patterns of shrew mandibles: do fragments tell the same story? J Archaeol Sci **53**:323–330.

Darvish J, Mohammadi Z, Mahmoudi A, Siahsarvie R (2014) Faunistic and taxonomic study of Rodents from northwestern Iran. IJAB **10**:119–136.

Djamali M, Beaulieu JL, Shah-hosseini M, Andrieu-Ponel V, Ponel P, Amini A, Akhani H, Leroy SAG, Stevens L, Lahijani H, Brewer S (2008) A late Pleistocene long pollen record from Lake Urmia, NW Iran. Quat Res **69**:413–420.

Drummond AJ, Rambaut A (2007) BEAST – Bayesian evolutionary analysis by sampling trees. BMC Evol Biol **7**:214.

Drummond AJ, Rambaut A, Shapiro B, Pybus OG (2005) Bayesian coalescent inference of past population dynamics from molecular sequences. Mol Biol Evol **22**:1185–1192.

Drummond AJ, Ho SYW, Phillips MJ, Rambaut A (2006) Relaxed phylogenetics and dating with confidence. PLoS Biol **4**:699–710.

Dubey S, Cosson JF, Magnanou E, Vohralik V, Benda P, Frynta D, Hutterer R, Vogel V, Vogel P (2007) Mediterranean populations of the lesser white-toothed shrew (Crocidura suaveolens group): an unexpected puzzle of Pleistocene survivors and prehistoric introductions. Mol Ecol **16**:3438–3452.

Elith J, Graham CH, Anderson RP, Dudik M, Ferrier S, Guisan A, Hijmans RJ, Huettmann F, Leathwick JR, Lehmann A, Li J, Lohmann LG, Loiselle BA, Manion G, Moritz C, Nakamura M, Nakazawa Y, Overton JMM, Peterson AT, Phillips SJ, Richardson K, Scachetti-Pereira R, Schapire RE, Soberon J, Williams S, Wisz M, Zimmermann N (2006) Novel methods improve prediction of species' distributions from occurrence data. Ecography **29**:129–151.

Elith J, Kearney M, Phillips S (2010) The art of modelling range-shifting species. Methods Ecol Evo **1**:330–342.

Ellerman JR (1966) The Families and Genera of Living Rodents / by J.R. Ellerman; with a List of Named Forms (1758-1936) by R. W. Hayman and G. W. C. Holt. Volume I. Rodents other than Muridae. Trustees of the British Museum (Natural History), London.

Ellerman JR, Morrison-Scott TCS (1951) Checklist of Palaearctic and Indian Mammals 1758 to 1946. Trustees of the British Museum (Natural History), London, p 810.

Etemad E (1978) Mammals of Iran. Vol. **I**, National Society for Protection of National Resources, Human and Environment Publications, Tehran 288. pp 182–192 (In Persian).

Evin A, Cucchi T, Cardini A, Vidarsdottir US, Larson G, Dobney K (2012) The long and winding road: Identifying pig domestication through molar size and shape. J Archaeol Sci **40**:735–743.

Excoffier L, Laval G, Schneider S (2005) Arlequin ver. 3.0: an integrated software package for population genetics data analysis. Evol Bioinform Online **1**:47–50.

Eygelis Yu K (1980) Rodents of Eastern Transcaucasus and the Problem of Sanitation of Local Plague Foci. Saratov University Press, Saratov (in Russian).

Fadda C, Corti M (2000) Three-dimensional geometric morphometrics of Arvicanthis: implications for systematics and taxonomy. J Zool Syst Evol Res **39**:235–245.

Fourcade Y, Engler JO, Rodder D, Secondi J (2014) Mapping species distributions with MAXENT using a geographically biased sample of presence data: a performance assessment of methods for correcting sampling bias. PLoS ONE **9**:e97122.

Fu YX (1997) Statistical tests of neutrality of mutations against population growth, hitchhiking and background selection. Genetics **147**:915–925.

Gholami Z, Esmaeili HR, Erpenbeck D, Reichenbacher B (2013) Phylogenetic analysis of Aphanius from the endorheic Kor River Basin in the Zagros Mountains, South-western Iran (Teleosti: Cyprinodontiformes: Cyprinodontidae). J Zoology Syst Evol Res **52**:130–141.

Goodwin GG (1939) Five New Rodents from the Eastern Elburz Mountains and a New Race of Hare from Teheran. Am Mus Nov 1950:1-5.

Goodwin GG (1940) Mammals collected by the legendre 1938 Iran expedition. Am Mus Novit **1802**:1–17.

Guindon S, Dufayard JF, Lefort V, Anisimova M, Hordijk W, Gascuel O (2010) New algorithms and methods to estimate maximum-likelihood phylogenies: assessing the performance of PhyML 3.0. Syst Biol **59**:307–321.

Gvozdik V, Moravec J, Klutsch C, Kotlik P (2010) Phylogeography of the Middle Eastern tree frogs (Hyla, Hylidae, Amphibia) as inferred from nuclear and mitochondrial DNA variation, with a description of a new species. Mol Phylogenet Evol **55**:1146–1166.

Habibi Kh (1977) The Mammals of Afghanistan: Their Distribution and Status. United Nations Development Programme, Food and Agriculture Organization of the United Nations and Department of Forests and Range, Ministry of Agriculture, Kabul.

Haddadian-Shad H, Darvish J, Rastegar-Pouyani E, Mahmoudi A (2016) Subspecies differentiation of the house mouse *Mus musculus* Linnaeus, 1758 in the center and east of the Iranian plateau and Afghanistan. Mammalia DOI: 10.1515/mammalia-2015-0041. accepted Jaunury 14, 2016.

Hall TA (1999) BioEdit: a user-friendly biological sequence alignment editor and analysis program for Windows 95/98. Nucl Acids Symp Ser **41**: 95–88.

Hasumi H, Emori S (2004) K-1 Coupled GCM (MIROC) Description, P. 34. K-1 Model Developers Tech Rep 1, Center for Climate System Research, University of Tokyo, Tokyo, Japan.

Hatt RT (1959) The Mammals of Iraq. Miscellaneous Publications Museum of Zoology, University of Michigan, 106: 89–90.

Hewitt G (1999) Post-glacial re-colonization of European biota. Biol J Linn Soc **68**:87–112.

doi: 10.1111/jzs.12145

Hewitt G (2000) The genetic legacy of the Quaternary ice ages. Nature **405**:907–913.
Hewitt G (2004) Genetic consequences of climatic oscillations in the Quaternary. Philos Trans R Soc B **359**:183–195.
Hijmans RJ, Cameron SE, Parra JL, Jones PG, Jarvis A (2005) Very high resolution interpolated climate surfaces for global land areas. Int J Climatol **25**:1965–1978.
Homke S, Verges J, Garces M, Emami H, Karpuz R (2004) Magnetostratigraphy of Miocene Pliocene Zagros foreland deposits in the front of the Push-e Kush Arc (Lurestan Province, Iran). Earth Planet Sci Lett **225**:397–410.
Jaeger JJ, Tong H, Denys C (1986) The age of the *Mus-Rattus* divergence: paleontological data compared with the molecular clock. ComptesRendus de l'Académie des Sciences Serie II Paris **302**:917–922.
James GA, Wynd JG (1965) Stratigraphic nomenclature of Iranian oil consortium agreement area. Am Assoc Petr Geol B **49**:2182–2245.
Kehl M (2009) Quaternary climate change in Iran-the state of knowledge. Erdkunde **63**:1–17.
Kimura M (1980) A simple method for estimating evolutionary rates of base substitutions through comparative studies of nucleotide sequences. Mol Evol **15**:111–120.
Krystufek B, Vohralik V (2009) Mammals of Turkey and Cyprus. Rodentia II: Cricetinae, Muridae, Spalacidae, Calomyscidae, Capromyidae, Hystricidae, Castoridae. University of Primorska, Science and research centre Koper, Koper.
Langgut D, Almogi-Labin A, Bar-Matthews M, Weinstein-Evron M (2011) Vegetation and climate changes in the South Eastern Mediterranean during the Last Glacial-Interglacial cycle (86 ka): new marine pollen record. Quat Sci Rev **30**:3960–3972.
Lay DM (1967) A study of the mammals of Iran. Fieldiana Zool **54**:1–282.
Librado P, Rozas J (2009) DnaSP v5: a software for comprehensive analysis of DNA polymorphism data. Bioinformatics **25**:1451–1452.
Macholan M, Mikula O, Vohralik V (2008) Geographic phenetic variation of two eastern-Mediterranean non-commensal mouse species, *Mus macedonicus* and *M. cypriacus* (Rodentia: Muridae) based on traditional and geometric approaches to morphometrics. Zool Anz **247**:67–80.
Marshall CR (1994) Confidence intervals on stratigraphic ranges: partial relaxation of the assumption of randomly distributed fossil horizons. Paleobiology **20**:459–469.
Montgelard C, Bentz S, Tirard C, Verneau O, Catzeflis FM (2002) Molecular systematic of Sciurognathi (Rodentia): the mitochondrial cytochrome b and 12S rRNA genes support the Anomaluroidea (Peptidae and Anomaluridae). Mol Phylogenet Evol **22**:220–233.
Mouthereau F, Tensi J, Bellahsen N, Lacombe O, De Bois grollier T, Kargar S (2007) Tertiary sequence of deformation in a thin-skinned/thick-skinned collision belt: the Zagros Folded Belt (Fars, Iran). Tectonics **26**:TC5006.
Musser GG, Carleton MD (2005) Superfamily Muroidea. In: Wilson DE, Reeder DM (eds), Mammal Species of the World, A Taxonomic and Geographic Reference, vol. **2**, 3rd ed. The Johns Hopkins University Press, Baltimore, pp 894–1531.
Neuhausee G (1936) The murids of Asia Minor. Plus much more. Translation from Russian.
Nicolas V, Schaeffer B, Missoup AD, Kennis J, Colyn M, Denys C, Tatard C, Cruaud C, Laredo C (2012) Assessment of three mitochondrial genes (16S, Cytb, CO1) for identifying species in the Praomyini tribe (Rodentia: Muridae). PLoS ONE **7**:e36586.
Paradis E, Claude J, Strimmer K (2004) APE: analyses of phylogenetics and evolution in R language. Bioinformatics **20**:289–290.
Pavlinov IY, Dubrovskyi YA, Rossolimo OL, Potapova EG (1990) Gerbils of the World's Fauna. Nauka Press, Moscow (in Russian).
PDB (2011) The Paleobiology Database. http://paleodb.org/cgi-bin/bridge.pl.
Phillips SJ, Dudik M (2008) Modeling of species distributions with Maxent: new extensions and a comprehensive evaluation. Ecography **31**:161–175.
Phillips SJ, Anderson RP, Schapire RE (2006) Maximum entropy modeling of species geographic distributions. Ecol Modell **190**:231–239.
Posada D, Crandall KA (2001a) comparison of different strategies for selecting models of DNA substitution. Syst Biol **50**:580–601.
Posada D, Crandall KA (2001b) Intraspecific gene genealogies: trees grafting into networks. Trends Ecol Evol **16**:37–45.
R Core Team (2014) R: A Language and Environment for Statistical Computing. R Foundation for Statistical Computing, Vienna, Austria. URL http://www.R-project.org/.
Rajaei ShH, Rödder D, Weigand AM, Dambach J, Raupach MJ, Wägele JW (2013) Quaternary refugia in southwestern Iran: insights from two sympatric moth species (Insecta, Lepidoptera). Org Divers Evol **13**:409–423.
Rambaut A, Suchard MA, Xie D, Drummond AJ (2013) Tracer v1.5. Available from http://beast.bio.ed.ac.uk/Tracer.
Ripley BD (1996) Pattern Recognition and Neural Networks. Cambridge University Press, Cambridge.
Roberts TJ (1977) The Mammals of Pakistan. Ernest Benn Limited, London.
Rogers AR, Harpending H (1992) Population growth makes waves in the distribution of pairwise genetic differences. Mol Biol Evol **9**:552–569.
Rohlf FJ (2013) TPSdig, v. 2.17. Stony Brook, Department of Ecology and Evolution, State University of New York, New York. http://life.bio.sunysb.edu/morph.
Rohlf FJ, Marcus LF (1993) A revolution in morphometrics. Trends Ecol Evol **8**:129–132.
Rohlf FJ, Slice D (1990) Extensions of the Procrustes method for the optimal superimposition of landmarks. Syst Biol **39**:40–59.
Schenk JJ, Rowe KC, Steppan Scott J (2013) Ecological opportunity and incumbency in the diversification of repeated continental colonizations by muroid rodents. Syst Biol **62**:837–864.
Schorr G, Holstein N, Pearman PB, Guisan A, Kadereit JW (2012) Integrating species distribution models (SDMs) and phylogeography for two species of Alpine Primula. Ecol Evol **2**:1260–1277.
Shahabi S, Aliabadian M, Darvish J, Kilpatrick CW (2013) Molecular phylogeny of brush-tailed mice of the genus *Calomyscus* (Rodentia: Calomyscidae) inferred from mitochondrial DNA sequences (Cox1 gene). Mammalia **77**:425–431.
Stöck M, Moritz C, Hickerson M, Frynta D, Dujsebayeva T, Eremchenko V, Macey JR, Papenfuss TJ, Wake DB (2006) Evolution of mitochondrial relationships and biogeography of Palearctic green toads (Bufo viridis subgroup) with insights in their genomic plasticity. Mol Phylogenet Evol **41**:663–689.
Stocklin J (1968) Structural history and tectonics of Iran; a review. Am Assoc Petroleum Geologists Bullet **52**:1229–1258.
Tabatabaei Yazdi F, Adriaens D (2011) Patterns of phenotypic skull variation in *M. persicus* (Rodentia: Muridae) in relation to geoclimatical conditions. IJAB **7**:129–142.
Tabatabaei Yazdi F, Adriaens D (2013) Cranial variation in *Meriones tristrami* (Rodentia: Muridae: Gerbillinae) and its morphological comparison with *Meriones persicus*, *Meriones vinogradov*i and *Meriones libycus*: a geometric morphometric study. J Zool Syst Evol Res **51**:239–251.
Tabatabaei Yazdi F, Adriaens D, Darvish J (2012) Geographic pattern of cranial differentiation in the Asian Midday Jird *Meriones meridianus* (Rodentia: Muridae: Gerbillinae) and its taxonomic implications. J Zool Syst Evol Res **50**:157–164.
Taberlet P, Fumagalli L, Wust-Saucy AG, Cosson JF (1998) Comparative phylogeography and postglacial colonization routes in Europe. Mol Ecol **7**:453–464.
Tajima F (1989) Statistical method for testing the neutral mutation hypothesis by DNA polymorphism. Genetics **123**:585–595.
Tamura K, Dudley J, Nei M, Kumar S (2007) MEGA4: molecular evolutionary genetics analysis (MEGA) software version 4.0. Mol Biol Evol **24**:1596–1599.
Thomas O (1920) Scientific Results of the Mammal Survey. No. XX. A. Some new mammals from Baluchistan and North-West India. B. Two new species of *Calomyscus*. J Bombay Nat Hist Soc **26**:933–940.
Varela S, Lima-Ribeiro MS, Terribile LC (2015) A short guide to the climatic variables of the last glacial maximum for biogeographers. PLoS ONE **10**:e0129037.

doi: 10.1111/jzs.12145

Venables WN, Ripley BD (2002) Modern Applied Statistics with S, 4th edn. Springer-Verlag, New York, p 495.
Warren DL, Glor RE, Turelli M (2010) ENM Tools: a toolbox for comparative studies of environmental niche models. Ecography **33**:607–611.
Zelditch ML, Swiderski DL, Sheets HD (2012) Geometric Morphometrics for Biologists: A Primer. Elsevier Academic Press, London.

Supporting Information

Additional Supporting Information may be found in the online version of this article:

Figure S1: Anatomical location of the 25 landmarks on the ventral view of *M. persicus* skull used in this survey.

Table S1: Definition and numbering of the landmarks (LM) digitized on the ventral view.

Table S2: Estimated classification for the discrimination between the 11 groups of *M. persicus* using the KNN method of classification.

doi: 10.1111/jzs.12145